Preadipocyte IL-13/IL-13Rα1 signaling regulates beige adipogenesis through modulation of PPAR gamma activity

Alexandra R. Yesian[1], Mayer M. Chalom[1,2], Nelson H. Knudsen[1,3], Alec L. Hyde[1], Jean Personnaz[1,4], Hyunjii Cho[1], Yae-Huei Liou[1], Kyle A. Starost[1], Chia-Wei Lee[1], Dong-Yan Tsai[5], Hsing-Wei Ho[5], Jr-Shiuan Lin[6], Jun Li[7], Frank B. Hu[7], Alexander S. Banks[8] and Chih-Hao Lee[1,5]

[1]Department of Molecular Metabolism, Harvard T.H. Chan School of Public Health, Boston, MA, USA

[2]Graduate School of Biomedical Sciences, Department of Cellular, Molecular, and Developmental Biology, Tufts University School of Medicine, Boston MA, USA

[3]Current address: Center for Cancer Research, Massachusetts General Hospital, Harvard Medical School, Charlestown, MA, USA; Broad Institute of Harvard and Massachusetts Institute of Technology, Cambridge, MA, USA

[4]Current address: RSD, Université de Toulouse, INSERM, INRAe, ENVT, UPS, Toulouse, France.

[5]Genomics Research Center, Academia Sinica, Taipei, Taiwan

[6]Graduate Institute of Immunology, National Taiwan University College of Medicine, Taipei, Taiwan

[7]Department of Nutrition, Harvard T.H. Chan School of Public Health, Boston, MA, USA[7]

[8]Division of Endocrinology, Diabetes and Metabolism, Beth Israel Deaconess Medical Center, Harvard Medical School, Boston, MA, USA

Authorship note: A.R.Y and M.M.C contributed equally to this work

Correspondence should be addressed: C.-H.L. e-mail: clee@hsph.harvard.edu, Department of Molecular Metabolism, Harvard T.H. Chan School of Public Health, 665 Huntington Ave, Boston, MA 02115, USA; clee2023@gate.sinica.edu.tw, Genomics Research Center, Academia Sinica, 128 Academia Rd, Sec 2, Nankang Dist., Taipei 115, Taiwan, (Tel) 886-2-2787-1200.

Conflict of interest: The authors have declared that no conflict of interest exists.

Abstract

Type 2 innate lymphoid cells (ILC2) regulate the proliferation of preadipocytes that give rise to beige adipocytes. Whether and how ILC2 downstream Th2 cytokines control beige adipogenesis remain unclear. We employed cell systems and genetic models to examine the mechanism through which interleukin-13 (IL-13), an ILC2-derived Th2 cytokine, controls beige adipocyte differentiation. IL-13 priming in preadipocytes drives beige adipogenesis by upregulating beige-promoting metabolic programs, including mitochondrial oxidative metabolism and PPARγ-related pathways. The latter is mediated by increased expression and activity of PPARγ through IL-13 receptor α1 (IL-13Rα1) downstream effectors, STAT6 and p38 MAPK, respectively. *Il13* knockout (Il13KO) or preadipocyte *Il13ra1* knockout (Il13ra1KO) mice are refractory to cold- or β-3 adrenergic agonist-induced beiging in inguinal white adipose tissue, whereas *Il4* knockout mice show no defects in beige adipogenesis. Il13KO and Il13ra1KO mouse models exhibit increased body weight/fat mass and dysregulated glucose metabolism but have a mild cold intolerant phenotype, likely due to their intact brown adipocyte recruitment. We also find that genetic variants of human *IL13RA1* are associated with body mass index and type 2 diabetes. These results suggest that IL-13 signaling-regulated beige adipocyte function may play a predominant role in modulating metabolic homeostasis rather than in thermoregulation.

Introduction

The maintenance of a healthy body mass index (BMI) throughout the lifespan is critical for prevention of the metabolic sequelae of obesity, including type 2 diabetes (T2D) (1). Relative to other fat depots, the subcutaneous white adipose tissue of humans exhibits a high degree of metabolic flexibility that plays a key regulatory role in weight gain and glucose homeostasis (2). The inguinal white adipose tissue (iWAT) of mice similarly exhibits high metabolic activity, in part because it is a primary source of thermogenic beige adipocytes that undergo uncoupling protein 1 (UCP1)-mediated uncoupled respiration upon sympathetic activation (2-4). In humans, the activity of thermogenic adipocytes is inversely associated with BMI and body fat percentage (5-7), and activation of these cells by β3-adrenergic agonists improves glucose tolerance in overweight patients (8). Studies have indicated that adult human thermogenic adipocytes may be more similar to murine beige adipocytes than murine brown adipocytes, making beige cells an appealing preclinical model for the development of new therapeutics (9, 10).

Inducible beige adipocytes initially develop via *de novo* adipogenesis, or recruitment (11-13). Although single-cell RNA sequencing studies have identified potential beige precursor populations (14-17), the delineation of factors that determine white versus beige adipocyte fate is ongoing. Several transcription factors and coactivators, such as PPARγ and PPARγ coactivator (PGC)-1α, have been implicated in both beige and brown adipogenic programs (18). The initiation of adipocyte differentiation requires activation of PPARγ, the master regulator of adipogenesis. In conventional preadipocyte cell models, such as 3T3-L1 cells that differentiate into large lipid droplet-filled mature adipocytes, *Pparg* expression can only be detected around the second day of a 6-day differentiation course (19). By contrast, *Pparg* has been identified as a marker of one beige precursor population, and activation of PPARγ by synthetic ligands has been shown to increase

beiging of white adipose tissues (20-22). Most beige adipogenesis appears to occur in early post-natal development (23-25), and the proliferative capacity of adipogenic progenitor cells declines rapidly in mice between 4-7 weeks of age (25). After undergoing adipogenesis, mature beige adipocytes may "whiten" over time, as decreased stimulation reduces their thermogenic activity (2); however, these cells maintain their beige identity and have the potential to be re-activated in adulthood (13, 26, 27).

The Th2 cytokines IL-4 and IL-13, which share a heterodimeric receptor complex of IL-4Rα and IL-13Rα1 (28), are classically implicated in the immune response to allergens and parasitic worms (29). In mice, Th2 signaling has been proposed to control the development of beige adipose tissue (25, 30, 31). Notably, Th2 cytokines and type 2 innate lymphoid cells (ILC2), which produce mainly IL-13 and IL-5, have been shown to regulate the proliferation of beige precursors in young mice and promote adaptive thermogenesis (25, 30). However, while one study suggests that the ILC2-Th2 cytokine axis regulates the proliferation of beige adipocyte progenitor cells and iWAT *Ucp1* expression in an IL-4Rα dependent manner (25), a second study demonstrates that adipose ILC2s promote beiging through the production of methionine-enkephalin (30). Thus, questions remain as to whether the cytokines downstream of ILC2 are involved in beige adipogenesis, as well as the mechanisms by which they regulate this process.

We have previously shown that IL-13 acts directly on tissues and cells to regulate metabolism (32, 33). During endurance exercise, ILC2-derived IL-13 and muscle IL-13Rα1 promote the adaptive metabolic response by enhancing mitochondrial biogenesis and oxidative metabolism (32). In line with the metabolic regulatory roles of IL-13 signaling, genome-wide association studies (GWAS) have identified *IL13RA1* as a top locus for BMI and type 2 diabetes (34, 35). In this study, we demonstrate that in addition to the reported function of Th2 cytokines

in beige precursor proliferation (25), activation of preadipocyte IL-13/IL-13Rα1 signaling drives beige adipogenesis in iWAT, in part through regulation of PPARγ expression and activity. This regulatory mechanism does not impact brown adipocyte recruitment and, as such, is not required for maintaining core body temperature. Disruption of preadipocyte IL-13 signaling leads to increased weight gain and insulin resistance, suggesting that IL-13/IL-13Rα1-regulated beige adipogenesis may function to modulate metabolic homeostasis. Our results also demonstrate that IL-4 is not required for cold-induced beige adipocyte recruitment, highlighting the importance of the ILC2-IL-13 axis in white adipose tissue beiging during cold challenge.

Results

IL-13 signaling mediates beige adipocyte recruitment

To examine the contributions of IL-13 signaling to thermogenesis in post-natal development, 8-week-old female wild-type (WT) and *Il13*-knockout (Il13KO) mice were subjected to a cold challenge. Il13KO mice exhibited a significant reduction in the core body temperature after 72 hours at 4°C (Figure 1A). Immunoblot analysis of iWAT revealed a defect in the induction of UCP1 and mitochondrial oxidative phosphorylation (OXPHOS) complex proteins in cold-exposed Il13KO mice, compared to WT controls (Figure 1B). Histology further demonstrated a reduction in adipocyte beiging in iWAT of cold-exposed Il13KO mice (Figure 1C). In contrast, there was no difference in tissue morphology or UCP1 protein expression in brown adipose tissue (BAT) of Il13KO mice (Supplemental Figure 1, A and B), indicating that the thermogenic defect at the later stage of the cold challenge was likely due to impaired beige adipocyte development.

Since previous studies have reported that Th2 cytokines directly promote the proliferation of beige progenitor cells (25), we set out to determine whether IL-13 exerts its effects through preadipocyte IL-13Rα1 signaling. Mice with a conditional *Il13ra1* allele (*Il13ra1*$^{f/f}$) were crossed to mice expressing a *Prx1*^{Cre} transgene to generate preadipocyte-*Il13ra1*-knockout (pIl13ra1KO) mice. *Prx1*^{Cre} has previously been validated for the study of preadipocytes (36). PCR analyses of genomic DNA validated *Il13ra1* gene deletion in iWAT (and primary inguinal adipocytes) and, to a lesser extent, in epididymal white adipose tissue (eWAT) and BAT of pIl13ra1KO mice (Supplemental Figure 1C). Young *Il13ra1*$^{f/f}$ (Control) and pIl13ra1KO male mice were subjected to a cold challenge. Similar to Il13KO mice, pIl13ra1KO mice exhibited a moderate defect in core body temperature maintenance and a reduction in iWAT UCP1 and OXPHOS proteins at 4°C

(Figure 1, D and E). The morphology of iWAT from cold-exposed pIl13ra1KO also showed impaired formation of multilocular beige adipocytes (Figure 1F). The BAT of pIl13ra1KO mice appeared fully functional, as evidenced by UCP1 immunoblot and histology (Supplemental Figure 1, D and E). In concert, decreased *Ucp1* and OXPHOS gene expression was observed in iWAT, but not BAT of pIl13ra1KO mice, despite the reduction in *Il13ra1* expression detected in both fat depots (Figure 1G and Supplemental Figure 1F). *Il13ra1* expression in the liver and muscle was comparable between control and pIl13ra1KO mice (Supplemental Figure 1G). Collectively, these results demonstrate that IL-13/IL-13Rα1 signaling in preadipocytes contributes to cold-induced recruitment of beige adipocytes.

IL-4 has also been implicated in beige adipogenesis (25). Splenocytes from *Il4*-knockout (Il4KO) mice failed to express *Il4* when stimulated with phorbol myristate acetate and ionomycin, while the expression of *Il13* was not affected (Supplemental Figure 2A). Unlike Il13KO mice, Il4KO mice exhibited no defects in body temperature maintenance after 72 hours at 4°C (Supplemental Figure 2B). In iWAT, the expression of *Ucp1* and OXPHOS and the formation of multilocular beige adipocytes were similar between WT and Il4KO mice (Supplemental Figure 2, C-E). Similarly, histological and expression analyses demonstrated that cold-induced browning of BAT was not affected in Il4KO mice (Supplemental Figure 2F and data not shown). To assess potential differences in temporal effects of IL-4 and IL-13 during cold-induced beige adipocyte recruitment, WT mice (7-8-week-old) were given antibodies against IL-13 or -IL-4 two hours before and 24 and 48 hours after initiation of a cold challenge. The short-term neutralizing antibody treatments did not affect cold tolerance over 72 hours (Supplemental Figure 2G), but anti-IL-13 significantly suppressed the upregulation of *Ucp1* and *Atp5k* by cold in iWAT, compared to control IgG treatment (Supplemental Figure 2H). Immunoblots and histology revealed that iWAT UCP1

and beige adipocyte recruitment were also blunted by anti-IL-13 treatment (Supplemental Figure 2, I and J). These effects were not observed with anti-IL-4 treatment, except for the significant reduction of cold-induced iWAT UCP1 protein. Both anti-IL-13 and anti-IL-4 treatments had no effect on brown adipocyte recruitment (Supplemental Figure 2K and data not shown). These findings suggest that IL-4 is not required for beige adipogenesis and highlight the importance of IL-13 in cold-induced beiging of iWAT in mice.

IL-13/IL-13Rα1 signaling in preadipocytes enhances the oxidative capacity of mature beige adipocytes

To investigate whether IL-13/IL-13Rα1 signaling in preadipocytes promotes beige adipogenesis, immortalized clonal preadipocyte cell lines were generated from the iWAT of WT mice. Several clonal cell lines were characterized, all of which shared similar responses to differentiation and IL-13 treatment. For subsequent studies, we focused on the WT clone #B6 preadipocytes (referred to as WT preadipocytes/cells), which differentiated robustly, with increasing expression of adipogenic and thermogenic markers over the course of 5-6 days (Supplemental Figures 3, A-B). The expression of *Il13ra1* declined after differentiation (Supplemental Figure 3C); similarly, *Il13ra1* expression was lower in primary adipocytes, compared to preadipocytes isolated from iWAT (Supplemental Figure 3D), indicating that IL-13Rα1 may have a predominant role in preadipocytes. We established stable shRNA-mediated *Il13ra1* knockdown (shIl13ra1) or control shRNA against luciferase (shLuc) in WT preadipocytes (Supplemental Figure 3E). Both stable lines differentiated comparably, as determined by Oil Red O staining, triglyceride (TG) content, and *Adipoq* gene expression, suggesting that *Il13ra1* is not required for adipocyte differentiation. (Supplemental Figures 3, F and H).

Preadipocytes were treated with IL-13 or vehicle for 24 hours before undergoing differentiation for 6 days. RNA-sequencing was performed on differentiated adipocytes (Figure 2A). Using an FDR threshold of <0.01, we identified 318 differentially expressed genes in mature adipocytes that received IL-13 pretreatment, compared to vehicle control (Supplemental dataset 1). To increase the power for gene enrichment analyses, the cutoff was reduced to a p-value of <0.01, which yielded 629 genes upregulated by IL-13 pretreatment. Functional annotation clustering performed using the Database for Annotation, Visualization, and Integrated Discovery (DAVID) (37, 38) revealed two major categories of upregulated genes – one involved in translation and ribosomal function, and another involved in mitochondrial function and respiration (Figure 2A and Supplemental Dataset 1). Within the mitochondrial category, we noted a subset of 42 genes in the KEGG thermogenesis pathway (Supplemental Dataset 1). A protein-protein interaction map generated using the STRING database demonstrated that the main cluster of the regulated genes included all five complexes of the mitochondrial electron transport chain (ETC) in the OXPHOS pathway and *Ucp1* (Figure 2B), suggesting that IL-13 treatment in the preadipocyte stage leads to differentiation towards a beige adipocyte-like phenotype. In fact, IL-13 priming was sufficient to increase levels of mitochondrial ETC complexes (Figure 2C) and upregulate UCP1 protein (Figure 2D) in differentiated adipocytes. The oxygen consumption rate (OCR) and phosphorylation of protein kinase A (PKA) substrates in response to stimulation with the β3-adrenergic agonist CL 316,243 (CL) were also higher in IL-13 primed adipocytes (Figure 2E and Supplemental Figure 3I). Regulation of mitochondrial function by IL-13 pretreatment was mediated by IL-13Rα1, as the induction of mitochondrial OXPHOS genes was lost in shIl13ra1 cells (Supplemental Figure 3J). RNA-seq analysis also identified 797 downregulated genes, with protein modification and

transcription comprising the major categories, including several homeobox genes known for their functions in development (Supplemental Dataset 1).

To examine the mechanism by which IL-13 acts in preadipocytes to regulate beige adipogenesis, we analyzed RNA-sequencing results in WT preadipocytes treated with IL-13 for 24 hours without differentiation. We identified 1875 genes significantly upregulated and 1797 genes significantly downregulated by IL-13 treatment in preadipocytes (FDR<0.01, Supplemental Dataset 2). Functional annotation clustering yielded similar results to the mature adipocyte analysis, with ribosomal and mitochondrial genes comprising the majority of upregulated categories (Figure 2F and Supplemental Dataset 2). Protein modification and transcription comprised most downregulated categories (Supplemental Dataset 2), including Notch signaling, which has been reported to suppress beige adipogenesis (39). The upregulated mitochondrial cluster included a subset of 81 genes in the KEGG thermogenesis pathway (Supplemental Dataset 2). The protein-protein interaction map identified three major clusters, including lipid metabolism (e.g., *Pnpla2*, *Mgll* and *Lipe*), G-protein coupled receptor (GPCR) signaling molecules (e.g. *Gnas, Adcy1*) that are also utilized by the β3-adrenergic receptor (ADRB3), as well as mitochondrial oxidative metabolism (e.g. *Ndufa1, Sdhb, Uqcrh, Cox6a1* and *Atp5k*, Figure 2G). IL-13 treated preadipocytes exhibited an increase in OXPHOS proteins (Figure 2H), an effect sustained throughout differentiation (Supplemental Figure 3K). IL-13 treatment also enhanced the OCR in preadipocytes (Figure 2I), and this effect was maintained two days after differentiation (Supplemental Figure 3L). IL-13 similarly induced the OCR in primary cells derived from the stromal-vascular fraction (SVF) of WT iWAT (Figure 2J). In support of these cell-based findings, expression of mitochondrial OXPHOS and lipid metabolism genes was downregulated in the iWAT of 8-week-old Il13KO mice compared to WT control mice (Figure 2K). To further examine

whether preadipocyte IL-13 signaling is important for cold-induced beige adipogenesis, control and whole-body *Il13ra1* knockout (Il13ra1KO) mice were exposed to 4°C for three days; primary preadipocytes were isolated from iWAT, followed by adipocyte differentiation for 6 days. Cold exposure enhanced expression of *Il13ra1* and *Ucp1* in differentiated WT adipocytes compared to the room temperature (RT) condition (Supplemental Figure 3M). By contrast, the expression of *Ucp1* was lower in differentiated Il13ra1KO adipocytes in both RT and cold-primed conditions compared to WT controls. These data indicate that preadipocyte IL-13 signaling drives differentiation into a highly oxidative beige adipocyte-like population.

IL-13 acts upstream of PPARγ to regulate beige adipogenesis

The three clusters of IL-13-regulated pathways in the protein-protein interaction map converged on PPARγ as a regulatory node (Figure 2G). In fact, the lipid metabolism cluster included several PPARγ target genes, such as *Lipe* (hormone sensitive lipase, HSL), *Pnpla2* (adipose triglyceride lipase, ATGL), *Mgll* (monoglyceride lipase), *Bscl2* (seipin), and *Abcd2*. We first validated that IL-13 treatment increased PPARγ protein in the WT preadipocyte cell line (Figure 2H) and in primary cells derived from the SVF of WT iWAT (Supplemental Figure 4A). To address potential clonal effects from the WT preadipocyte cell line and assess the role of IL-13Rα1 in the control of *Pparg* expression, preadipocyte clonal cell lines were also generated from the iWAT of Il13ra1KO mice. Multiple Il13ra1KO preadipocyte clones were characterized, and the KO clone #1.5 cell line was utilized to generate a transgenic *Il13ra1*-reexpression cell line (Il13ra1RE) for rescue studies (Supplemental Figure 4B). Il13ra1RE cells differentiated comparably to controls with pBabe empty vector (Il13ra1KO control, Supplemental Figure 4, C and D). While IL-13 was ineffective in Il13ra1KO cells, the regulation of *Pparg* and its

downstream targets was restored in the Il13ra1RE preadipocytes, demonstrating that induction of the PPARγ pathway by IL-13 was IL-13Rα1-dependent (Figure 3, A and B). Of note, preadipocytes only express *Pparg1*; expression of *Pparg2* is detectable at the later stage of adipocyte differentiation and is lower than that of *Pparg1* (not shown). We obtained the same RT-qPCR results using primer pairs for *Pparg1* or *Pparg* (common region for *Pparg1* and *Pparg2*).

Activation of PPARγ by high-affinity ligands such as rosiglitazone (rosi) promotes beige adipogenesis both *in vivo* and in cultured adipocytes (20, 21, 40-43). To explore the IL-13-PPARγ axis in beige adipogenesis, preadipocytes were treated with vehicle, IL-13, rosi, or a combination of IL-13 plus rosi (IL-13+rosi) for 24 hours. Rosi treatment had no effect on *Pparg* gene expression but induced the expression of PPARγ target genes to a much greater degree than IL-13 treatment (Figure 3C), which was expected from a potent PPARγ agonist. However, IL-13+rosi treatment resulted in significantly higher expression of PPARγ target genes compared to rosi alone. This effect persisted after switching to differentiation medium (containing dexamethasone, insulin, and IBMX) for 2 days (Figure 3D). A similar result was observed for the expression of *Adrb3*, consistent with the increased CL-triggered OCR and signaling observed in mature adipocytes primed with IL-13 (Figure 2E and Supplemental Figure 3I). Furthermore, mature adipocytes that received IL-13+rosi priming expressed higher levels of UCP1 and ADRB3 proteins than rosi treatment alone (Figure 3E). Thus, rosi priming in preadipocytes is sufficient to promote beige adipogenesis, and IL-13 potentiates PPARγ-mediated differentiation of beige adipocytes with enhanced β3-adrenergic signaling.

The effect of rosi+IL-13 on PPARγ target gene expression could be explained by the ~2-fold increase in *Pparg* expression by IL-13 (Figure 3C and Supplemental Figure 4A). However,

the regulation for some genes, notably *Abcd2*, appeared to be synergistic. This prompted us to investigate whether IL-13/IL-13Rα1 signaling further modulates PPARγ activity. To examine this potential mechanism, we overexpressed *Pparg1* in WT preadipocytes (Pparg1OE). In the pBabe empty vector control cells, IL-13 treatment significantly induced *Pparg* gene expression (Supplemental Figure 4E). Pparg1OE preadipocytes had higher *Pparg* gene expression under unstimulated conditions, which did not further increase with IL-13 treatment. However, Pparg1OE cells treated with IL-13+rosi still expressed higher levels of PPARγ target genes compared to rosi alone, suggesting that IL-13 signaling may also enhance PPARγ activity in preadipocytes (Supplemental Figure 4F). To quantitatively assess PPARγ transcriptional activity, we transfected Pparg1OE preadipocytes with a PPAR response element (PPRE)-luciferase reporter construct. The cells were treated with vehicle control, IL-13, rosi, or IL-13+ rosi for 24-hours. PPRE activity was significantly higher in IL-13+rosi-treated cells compared to cells treated with rosi alone (Supplemental Figure 4G). Using a mammalian one-hybrid system, in which the PPARγ ligand binding domain (LBD) was fused to yeast Gal4 DNA binding domain (Gal4BD-PPARγ-LBD, Figure 3F), we demonstrated that IL-13 similarly enhanced rosi-induced PPARγ transactivation of the luciferase reporter activity in WT preadipocytes. Of note, IL-13 alone did not affect PPARγ activity, indicating that IL-13 treatment does not lead to the production of endogenous PPARγ ligands. In line with a nonessential role for IL-4 in beige adipogenesis, IL-4 treatment in preadipocytes failed to increase mitochondrial respiration and to potentiate the effects of rosi on regulation of *Lipe* expression and Gal4BD-PPARγ-LBD transactivation activity (Supplemental Figures 4, H-J).

Chromatin immunoprecipitation (ChIP) on the promoters of two PPARγ target genes, *Lipe* and *Mgll*, was performed to examine PPARγ DNA binding activity. We identified two potential

PPREs (designated as C1 and C2) within 1.3 kb promoter region of the *Lipe* gene (Figure 3G, left panel). The upstream C1 site, but not the downstream C2 site, showed similar PPARγ binding at day 3 of differentiation in rosi or IL-13+rosi primed cells (Figure 3G). However, rosi priming increased the signal of acetyl-histone H3, Lys27 (H3ac) on both C1 and C2 sites after the overnight treatment, and to a greater extent on day 3 of differentiation, which was further enhanced by IL-13+rosi cotreatment. For the *Mgll* gene, two adjacent PPREs were identified at around 2.5 kb of the 5' promoter region (Supplemental Figure 4K, upper panel). PPARγ binding was similarly detected on both sites on day 3 of differentiation in rosi or IL-13+rosi primed cells (Supplemental Figure 4K). IL-13+rosi also induced a stronger effect than rosi alone on increasing H3ac signal in ChIP. Collectively, these results suggest that IL-13 does not affect PPARγ ligand production or DNA binding, but instead may modulate PPARγ transcriptional activity, likely through coactivator-mediated regulation of the chromatin landscape.

IL-13-IL-13Rα1 potentiates PPARγ transcriptional activity through p38 MAPK

PGC-1α, a well-established PPARγ coactivator and beige adipocyte regulator, can be activated by p38 mitogen-activated protein kinase (MAPK) in response to inflammatory cytokines (44). IL-13 has been shown to activate p38 MAPK in immune cells (45). In preadipocytes, IL-13 induced the phosphorylation of p38 MAPK at a comparable time course as the toll-like receptor 4 ligand lipopolysaccharide (LPS, Supplemental Figure 5A). To assess whether IL-13 could increase PPARγ activity through the p38-MAPK-PGC-1α axis, we continued our studies in AD293 cells because of their low background PPARγ activity. In AD293 cells, *Ppargc1* co-transfection dose-dependently enhanced the activity of PPARγ-LBD even in the absence of rosi, and this effect was blunted by SB 203580, a p38 MAPK inhibitor (p38i) (Figure 4A). In addition, IL-13 significantly

increased PGC-1α mediated PPARγ-LBD activity, an effect abolished by p38i (Figure 4B). Similar results were obtained in WT preadipocytes (Supplemental Figure 5B). In the presence of p38i, IL-13 still significantly induced *Pparg* gene expression (Supplemental Figure 5C). However, gene expression analyses in WT cells demonstrated that p38i blocked the potentiation activity of IL-13+rosi cotreatment on PPARγ target genes (Figure 4, C and D). This inhibitory effect of p38i treatment in preadipocytes persisted 3 days after differentiation (Supplemental Figure 5D).

STAT6, the canonical downstream regulator of Th2 cytokines, increases *Pparg* expression in macrophages (46, 47). In preadipocytes, IL-13 robustly induced phosphorylation of STAT6 (Supplemental Figure 5A). Treatment with AS1517499, a STAT6 inhibitor (STAT6i), blocked the induction of *Pparg* expression by IL-13 (Supplemental Figure 5E). STAT6i also significantly reduced the expression of PPARγ target genes (Figure 4, E and F), an effect maintained after 3 days of differentiation (Supplemental Figure 5F). STAT3 has also been shown to regulate oxidative metabolism downstream of IL-13 in muscle (32). In preadipocytes, IL-13 was able to increase STAT3 phosphorylation, which appeared to decline quickly compared to phospho-STAT6 (Supplemental Figure 5G). Treatment with a STAT3 inhibitor (Stattic, STAT3i) failed to inhibit the IL-13-mediated increase in PPARγ target gene expression (Supplemental Figure 5H), indicating that STAT3 is not a primary mediator of IL-13 signaling in preadipocytes.

Consistent with the gene expression result, rosi+IL-13 cotreatment induced HSL protein to a greater extent than rosi in WT preadipocytes (Figure 4G). p38i co-treatment reduced the induction of HSL protein by IL-13. Furthermore, differentiated adipocytes primed with IL-13+rosi expressed higher levels of UCP1 and UQCRC2 (OXPHOS complex III) proteins compared to rosi alone (Supplemental Figure 5I), and the effect of IL-13 was blunted by p38i co-treatment. STAT6i similarly suppressed HSL protein expression (Figure 4H). In addition, STAT6i treatment in

preadipocytes completely blocked differentiation (data not shown), likely due to PPARγ inhibition. Collectively, these data indicate that intact PPARγ signaling in preadipocytes plays an important role in beige adipogenesis, and IL-13 promotes beige adipocyte differentiation by modulating both the expression and the activity of PPARγ through the STAT6 and p38 pathways, respectively.

IL-13/IL-13Rα1 signaling in mature adipocytes is not required for thermogenesis

Previous studies have demonstrated that beige precursor cells decline in adult mice (25). Thus, we investigated the effects of IL-13 deficiency on the thermogenic competence of adult mice, which revealed no difference in the body temperature between WT and Il13KO mice at thermoneutrality, 22°C or 4°C (Supplemental Figure 6A). However, Il13KO mice ate significantly more at 4°C in the light cycle. Similar results were observed in Il13ra1KO mice (Supplemental Figure 6B). The increased food intake may indicate a compensatory effect to maintain body temperature and suggests that IL-13/IL-13Rα1 may still modulate beige adipocyte function in adult mice. To test this possibility, we pharmacologically activated the beige/brown adipogenic program by dosing WT and Il13KO mice with CL for 10 days. Histology demonstrated that Il13KO mice had larger adipocytes in iWAT under unstimulated conditions and showed impaired formation of multilocular adipocytes in response to CL (Figure 5A). Immunoblots also revealed a diminished induction of UCP1 in response to CL in the iWAT of Il13KO animals (Figure 5B). Consistent with findings in young mice, histological and immunoblot analyses of BAT revealed no difference in tissue morphology or UCP1 expression between CL-injected WT and Il13KO mice (Supplemental Figure 6, C and D). Il13ra1KO mice exhibited a similar defect in CL-induced beige adipocyte recruitment and UCP1 protein expression (Figure 5, C and D).

The attenuated response to CL in adult Il13KO and Il13ra1KO mice could be due to two non-mutually exclusive scenarios: decreased beige adipogenesis in post-natal development,

resulting in a smaller population of mature cells to be activated in adulthood, or decreased beige adipocyte activation due to loss of IL-13 signaling in mature adipocytes. To clarify the role of IL-13 in promoting beige cell activation, we generated mature beige/brown adipocyte-*Il13ra1*-knockout (bIl13ra1KO) mice by crossing *Il13ra1*$^{f/f}$ mice with *Ucp1*^{Cre} mice. We detected the deleted *Il13ra1* genomic DNA in iWAT and BAT and the deletion was further enhanced by cold exposure, in which *Ucp1* was expected to be highly induced (Supplemental Figure 6E). A reduction in *Il13ra1* mRNA expression was detected in mature adipocytes, but not SVF from iWAT, indicating the bIl13ra1KO model left preadipocyte IL-13 signaling intact (Supplemental Figure 6F). In line with this notion, we found that 6-week-old bIl13ra1KO mice had no defect in thermogenesis after 72 hours at 4°C, compared to control *Il13ra1*$^{f/f}$ mice (Supplemental Figure 6G). There was also no difference in tissue morphology of iWAT and BAT between control and bIl13ra1KO mice upon cold exposure (Supplemental Figure 6, H and I).

In 5-month-old control mice, a 7-day CL treatment induced the formation of multilocular beige adipocytes and increased UCP1 protein levels in iWAT (Figure 5, E and F). These responses appeared to be reduced in bIl13ra1KO mice, though to a lesser extent than Il13KO, Il13ra1KO and pIl13ra1KO mice. To further examine the CL/β3-adrenergic response, iWAT fat pads from control and bIl13ra1KO mice were stimulated with CL ex vivo. Immunoblotting confirmed that the induction of both phospho-PKA substrates and phospho-HSL by CL was reduced in the bIl13ra1KO fat pads compared to those from control mice (Figure 5G). Collectively, these results suggest that while IL-13/IL-13Rα1signaling may serve a functional role in UCP1-positive mature adipocytes from iWAT, IL-13 exerts its beige adipocyte-promoting activity primarily in preadipocytes.

The *Il13ra1* gene is associated with body weight and glucose metabolism

In a large-scale GWAS from Biobank Japan (34, 35), variants of *IL13RA1* were significantly associated with BMI and T2D (Supplemental Figure 7, A and B). Genetic variants at the *IL13RA1* locus were also associated with BMI in the Genetic Investigation of Anthropomorphic Traits (GIANT) Consortium (a multi-ethnic group comprised of 62.2% Europeans, 16.4% Hispanic/Latin American, 15.3% Asian and 6.1% African American/Afro-Caribbean, Figure 6A) (48); however, the same locus was not associated with T2D in the predominately European population (data not shown) (49). Variants located on *IL13RA2* (a decoy receptor for IL-13) or *IL4R* were not associated with BMI or T2D (Supplemental Figure 7, C and D, and data not shown). Expression levels of human *IL13RA1* were higher in subcutaneous fat, compared to visceral fat, liver, and muscle (50) (Figure 6B).

In mice, loss of *Il13ra1* resulted in increased body weight and significantly heavier iWAT fat pads, compared to WT mice (Figures 6, C and D). Il13ra1KO mice were also more glucose intolerant (Figure 6E). A similar phenotype was observed in pIl13ra1KO mice, compared to control mice (Figure 6, F-H). Given the relatively minor role of IL-13/IL-13Rα1 signaling in mature adipocytes, the fat mass and glucose tolerance findings in bIl13ra1KO mice were unsurprisingly less profound compared to pIl13ra1KO or Il13ra1KO mice (Supplemental Figure 7, E-G). These data suggest that IL-13/IL-13Rα-mediated beige adipocyte function may play a regulatory role in weight maintenance and metabolic homeostasis.

Discussion

Using multiple mouse models and cell systems, we demonstrate that preadipocyte IL-13/IL-13Rα1 signaling is required for beige adipogenesis. IL-13 priming in preadipocytes is sufficient to drive the development of highly oxidative beige adipocytes, and the effects of IL-13 pretreatment are maintained throughout differentiation. PPARγ acts as one of the major downstream effectors of IL-13/IL-13Rα1 signaling; IL-13 increases the expression of PPARγ through STAT6 and enhances PPARγ activity by p38 MAPK-mediated PGC-1α co-activation. Despite its role in regulating beige adipogenesis, deletion of IL-13 signaling, either through *Il13* or *Il13ra1* gene deletion, yields a moderate defect in thermogenesis. This is consistent with another report suggesting that the thermogenic capacity of beige adipocytes in iWAT represents ~10% that of the brown adipocytes in C57BL/6 mice (51). Our published work on Il13KO (33) and the current study demonstrate that mice lacking whole-body or preadipocyte IL-13/IL13Rα1 signaling show increased weight gain and glucose intolerance. These findings thus uncouple the thermogenic and metabolic functions of IL-13-regulated beige adipogenesis.

Th2 cytokines have been reported to promote beige cell development by enhancing the proliferation of PDGFRα^{+} adipocyte progenitors (25). Due to the limited quantity of progenitors, characterizing the mechanistic role of Th2 signaling in beige adipogenesis has been challenging. Through the development of immortalized cell lines from iWAT, our study identifies an additional role for IL-13 in promoting the commitment of preadipocytes to beige adipocyte differentiation. IL-13 priming enhances oxygen consumption and OXPHOS complex protein expression in both preadipocytes and mature adipocytes. We have previously demonstrated that IL-13 controls muscle mitochondrial biogenesis and oxidative metabolism in response to endurance exercise training (32), suggesting that mitochondrial function is a primary target of IL-13 signaling. While STAT3 appears

to mediate the effect of IL-13 in muscle, IL-13 regulates beige adipogenesis partly through STAT6 and PPARγ. Previous studies have identified *Pparg* as a marker for beige preadipocytes (22). In conventional preadipocyte cell models, such as 3T3-L1 cells, *Pparg* expression is induced two days after initiation of differentiation (19). The iWAT-derived preadipocyte cell lines established in the current study express *Pparg* at an appreciable level in the undifferentiated state and these cells differentiate robustly to become mature adipocytes with small lipid droplets and elevated mitochondrial OXPHOS protein levels (Supplemental Figure 3). In addition, treatment with rosi or IL-13+rosi for 24 hours in preadipocytes is sufficient to promote differentiation into *Ucp1*-expressing adipocytes (Figure 3E). These observations suggest that preadipocyte PPARγ expression and activity play an important role in beige adipogenesis.

PPARγ agonists, such as rosi, have been used to induce beiging in cell and mouse studies. Since PPARγ is required for differentiation of all types of adipocytes, how does PPARγ activation exert the observed beiging effect? It is possible that modulation of PPARγ activity by transcriptional cofactors also contributes to beige adipogenic capacity (18). For instance, PGC-1α, originally identified as a PPARγ co-activator, has been shown to drive thermogenic gene expression and promote mitochondrial biogenesis in multiple tissues (52). In adipose tissue, deletion of PGC-1α results in a decrease in thermogenic and oxidative gene expression in iWAT, but not BAT (53). We find that in preadipocytes, IL-13 not only up-regulates PPARγ gene/protein expression but also increases its activity. The latter only requires the PPARγ ligand binding domain (LBD) where ligand-induced coactivator recruitment occurs. In the presence of PGC-1α, IL-13 further increases PPARγ LBD activity in a reporter assay. We identify p38 MAPK as a downstream effector of IL-13-IL-13Rα1 signaling mediating PCG-1α activation. p38 MAPK activation by cold and β3 adrenergic stimulation has previously been identified as a regulator of *Ucp1* expression in BAT, and this effect

was dependent on PGC-1α (54). Indeed, pharmacological inhibition of p38 blocks the ability of IL-13 to enhance PGC-1α coactivation of the PPARγ LBD. Similarly, p38 inhibition abrogates the synergistic effect of IL-13 and rosi cotreatment on PPARγ target gene expression in preadipocytes. Furthermore, "translation" is one of the top pathways upregulated by IL-13 treatment, which contains many ribosomal genes (Supplemental Dataset 2). In concert, the induction of HSL protein by IL-13 in the presence of rosi (Figure 4G) is higher than the increase in *Lipe* mRNA (which encodes HSL, Figure 4D), suggesting that IL-13 could regulate PPARγ targets through post-transcriptional regulation.

While previous work has demonstrated that both IL-4 and IL-13 promote the proliferation of beige precursors (25), Il4KO mice show no defect in cold-induced beige adipocyte recruitment in iWAT, suggesting that IL-4 is sufficient but not required for beige adipogenesis. It is also possible that within the first three days at 4°C, ILC2s and ILC2-derived IL-13 are the primary regulators of beige adipocyte differentiation, while IL-4 and IL-4 producing cells, such as eosinophils, may become important after prolonged cold exposure. Our results indicate that the relevance of IL-13-regulated beige adipocyte recruitment in thermogenesis in young mice becomes evident only after prolonged cold exposure. Previous studies have indicated that Th2 cytokines are dispensable for thermogenesis in adult mice (25). Consistent with these reports, 20-week-old mice lacking the IL-13/IL-13Rα1 pathway have no thermogenic defect, although these mice still have a blunted induction of beiging in response to β3-adrenergic stimulation. IL-13 signaling does not affect brown adipocyte function. It is possible the intact BAT activity is sufficient to maintain core body temperature in Il13KO, Il13ra1KO and pIl13ra1KO mice. Interestingly, these mice gain more weight and have impaired glucose intolerance compared to control mice. These results seem to disassociate the thermogenic and metabolic effects of IL-13 signaling mediated beige adipogenesis. The

metabolic phenotypes are less evident in bIl13ra1KO mice, which have *Il13ra1* gene deleted in *Ucp1*-expressing mature adipocytes, suggesting that IL-13 acts primarily in preadipocytes to regulate metabolism. Consistent with the observations in our mouse genetic models, genetic variants of the human *IL13RA1* gene have been shown to be associated with T2D and BMI in a Japanese population and with BMI in a predominately European population.

The human *PPARG* gene is among the first identified to associate with T2D and BMI (55, 56). PPARγ agonists are powerful anti-diabetic medications; however, existing drugs that target PPARγ have undesirable side effects, including weight gain and bone resorption (57, 58). A recent mouse study demonstrated that genetic overexpression of preadipocyte PPARγ in the early post-natal period is protective against the development of glucose intolerance later in life, providing evidence that the regulation of preadipocyte PPARγ is worthy of mechanistic investigation (59). Although our data supports the notion that PGC-1α coactivation is important for mediating the beige adipogenic process, it is possible that other transcriptional regulators and/or post-translational modifications of PPARγ may also be involved in the effects downstream of IL-13/IL-13Rα1. Future studies aiming to improve understanding of additional levels of regulatory mechanisms by the preadipocyte IL-13-PPARγ axis may help the development of more targeted therapeutics.

Methods

Sex as a biological variable. Our study examined male and female animals, and similar findings are reported for both sexes.

Animal studies. Mice were housed in a barrier facility with a 12-hour light/dark cycle and ad libitum access to chow (Mouse Diet 20 5058, PicoLab) and water. Il13KO mice on the Balb/c background were backcrossed to C57BL/6J mice (JAX) as previously described (33). The generation of the Il13ra1KO line was previously described (32). To obtain conditional knockout mice, the artificial exon acceptor sequences of the *Il13ra1*$^{-/-}$ allele were removed by crossing to the flipase transgene; these mice were used to generate cell type-specific knockouts. Il4KO mice (KN2: knockin huCD2) in the C57BL/6J background were generated by replacing the first two exons of *Il4* with a human CD2-encoding sequence (60) provided by Dr. Jr-Shiuan Lin.Prx1-Cre mice (JAX, Strain #005584) and Ucp1-Cre mice (JAX, Strain #024670) were used to generate pIl13ra1KO and bIl13ra1KO mice, respectively. The Prx1-Cre strain (61) and the Ucp1-Cre strain (62) have been characterized previously. A complete list of animal cohorts is found in Supplemental Table 1.

Cold exposure. Mice were transferred from 22°C and single-housed at 4°C for 72-hours with 12-hour light and dark cycles and ad libitum access to chow and water. Body temperatures were assessed using a rectal probe thermometer at baseline (22°C), and following 2, 4, 6, 24, 48, and 72-hours at 4°C. For neutralizing antibody experiments (63), mice were i.p. injected with anti-IL-13, anti-IL-4, or isotype IgG control at 100 μg/animal 2 hours before cold exposure. Two

additional doses at 50 μg were given 24 and 48 hours after cold exposure. Tissue was harvested at 72 hours.

Adipocyte cell line development and culture. Primary SVF was harvested from inguinal fat pads of WT and Il13ra1KO mice as described below. Preadipocytes were immortalized by retroviral infection with SV40 Large T antigen and maintained in high-glucose (4.5 g/L) Dulbecco's Modified Eagle Medium (DMEM, Corning) containing 10% FB Essence (Avantor) and penicillin-streptomycin (Corning). Multiple clonal cell lines were characterized in both the WT and Il13ra1KO backgrounds. To generate stable knockdown cell lines, shRNA for *Il13ra1* was cloned into the pSIREN-RetroQ vector and transfected into Phoenix packaging cells to produce retrovirus. Selection was with 3 μg/mL puromycin. The same protocol was used to generate stable overexpression cell lines for *Il13ra1* and *Pparg1* in the pBabe vector.

Preadipocytes were plated at a density of $5x10^4$ per well (12-well plates) for overnight and treated with 10 ng/mL recombinant mouse IL-13 (or IL-4, R&D Biosystems), 1 μM rosiglitazone (rosi, Sigma Aldrich), or a combination of IL-13 (10 ng/mL) + rosi (1 μM) for 24 hours. p38-MAPK inhibitor SB203580 (Abcam), STAT6 inhibitor AS1517499 (Selleck Chem) and STAT3 inhibitor Stattic (Abcam) were suspended in DMSO and administered at a concentration of 10 μM and 1 μM, respectively.

Two methods were used to differentiate preadipocytes: Preadipocytes were differentiated in high-glucose DMEM, 10% FBS (Gemini Bio-Products) with a complete cocktail of 5 μg/ml insulin from bovine pancreas (Sigma-Aldrich), 1 μM rosi, 0.5 mM 3- isobutyl-10-methylxanthine (IBMX, Sigma-Aldrich), and 1 μM dexamethasone (dex) for two days, followed by maintenance media containing 5 μg/ml insulin and 1 μM rosi for 4 days; or following priming with 1 μM rosi

for 24-hours, cells were differentiated in a cocktail of 5 μg/ml insulin, 0.5 mM IBMX, and 1 μM dex for two days, followed by maintenance media containing 5 μg/ml insulin for 4 days.

RNA-sequencing and analysis. RNA-seq studies were conducted in two different immortalized clonal cell lines with similar results. RNA-sequencing was performed on 4 replicates per condition (preadipocyte + vehicle, preadipocyte + IL-13, mature adipocyte + vehicle pretreatment, or mature adipocyte + IL-13 pretreatment). Sequencing, data processing and preliminary analyses were conducted at the IMB Genomics Core and IMB Bioinformatics Service Core at the Academia Sinica (Taipei, Taiwan) as described previously (32, 64): Briefly, samples were quantified with Ribogreen (Life Technologies, CA) and RNA integrity was checked with a Bioanalyzer 2100 (Agilent, CA) (RIN>8; OD 260/280 and OD 260/230>1.8). RNA libraries were prepared with the TruSeq Stranded mRNA Library Preparation Kit (Illumina). Sequencing was analyzed with an Illumina NextSeq 500. Raw data was analyzed using the CLC Genomics Workbench. A p-value cutoff of 0.01 and an FDR p-value of 0.01 were used for analyses of mature adipocytes and preadipocyte studies, respectively. Gene ontology analysis was performed using DAVID (37, 38). Protein-protein interaction maps were generated using the STRING Database (65).

Primary preadipocyte isolation and culture. Inguinal fat pads with lymph nodes excised were minced and transferred to a digestion buffer containing high-glucose DMEM with 2% BSA and 2 mg/ml collagenase II (Gibco). Following tissue digestion with mechanical disruption for 1 hour at 37°C, the digestion media was filtered through 70 or 100-micron mesh to remove debris. The cell suspension was pelleted by centrifugation. Mature adipocytes on the top layer were collected for separate assays. The remaining SVF was resuspended in ACK buffer to lyse red blood cells,

washed with DMEM, and resuspended in cell culture media containing high-glucose DMEM with 10% FB Essence and penicillin-streptomycin. Cells were expanded in 10 cm cell culture plates for 3 days before transferring to 12-well plates for experiments.

Mitochondrial respiration. Measurement of oxygen consumption rate (OCR) was performed using a Seahorse XF24 Bioanalyzer. Preadipocytes were plated in XF24 microplates at a density of $2x10^4$ per well to attach overnight. Cells were treated with mouse recombinant IL-13 (or IL-4) at a dose of 10 ng/mL or vehicle control for 24hours. An hour before the assay, cells were washed twice with PBS and changed to media containing minimal DMEM, 5mM glucose, and 1mM sodium pyruvate. Basal respiration was measured 3 times. Cells were then treated with oligomycin (2 μM), FCCP (1 μM), and rotenone + antimycin A (1 μM). Measurements were recorded 3 times following each injection. OCR was normalized to total protein content. The same protocol was carried out on day 3 of differentiating adipocytes.

For day 5 OCR analyses, preadipocytes were plated in a 6-well plate and treated with rosi (1 μM) or a combination of IL-13 (10 ng/mL) and rosi (1 μM) for 24 hours. Cells were washed and differentiated for 2 days in complete media containing a cocktail of insulin, IBMX, and dex. Cells were then re-plated in XF24 microplates at a density of $1.5x10^4$ per well. Differentiation was continued in complete media containing insulin for days 2 through 5. One hour before the assay, cells were treated as described above. CL was injected at a final concentration of 2 μM, followed by treatments with oligomycin (4 μM), FCCP (2 μM), and rotenone + antimycin A (1 μM). OCR was normalized to total protein content for each well.

Gene expression. RNA was isolated from cells using the NucleoSpin RNA Plus kit (Macherey-Nagel), and from tissue using Trizol. Reverse transcription of isolated RNA was performed using the Verso cDNA synthesis kit (Thermo Fisher Scientific). RT-qPCR using SYBR green (SMOBio) was performed to quantify gene expression. Gene expression was normalized to a standard curve and presented as expression relative to *36b4*. Primer sequences are listed in Supplemental Table 2.

Immunoblotting. Protein quantification of cell and tissue lysates was performed using a BCA kit (Pierce). Proteins were separated by SDS-PAGE, transferred onto PVDF membranes, and incubated in primary antibody overnight at 4°C in TBST with 1% BSA. Primary antibodies are listed in Supplemental Table 3. The BioRad ChemiDoc XRS+ imaging system was used to detect ECL signal. Quantification of immunoblot results was performed using ImageJ.

Reporter assays. For PPAR response element (from *Acox1* gene promoter) reporter assays, *Pparg1OE* preadipocytes cultured in 10 cm plates were transfected with the PPRE reporter construct at a concentration of 10 μg/10^6 cells for 24 hours, re-plated on 24-well plates (~$4x10^4$ cells/well), and treated overnight with IL-13, rosi, or IL-13+rosi. Cells were lysed using a passive lysis buffer (Promega) and the Luciferase Assay System (Promega) was used to quantify luciferase activity, which was normalized to protein content to obtain relative luciferase units (RLU). To assess PPARγ-LBD activity, WT preadipocytes were co-transfected in 10 cm plates with the Gal4 binding site-containing reporter (10 μg) and either Gal4BD Control or Gal4-PPARγ-LBD (2.5 μg). Twenty-four hours after transfection, each plate was split into two 10 cm plates and transfected overnight with either CMV vector control or *Ppargc1* expression vector (2.5 μg) before plating in

24-well or 48-well plates. After attaching, cells were treated with IL-13, rosi, or rosi+IL-13 ± P38 inhibitor overnight. In certain experiments, IL-4 treatment was included. The reporter luciferase activity was normalized to protein content for RLU. For AD293 cells, co-transfection was conducted directly in 96-well plates. A β-galactosidase reporter was included for normalization for RLU (50 ng for reporters and up to 10 ng for each expression vector).

Chromatin Immunoprecipitation (ChIP). Assessments of PPARγ promoter occupancy and histone H3 Lysine 27 acetylation (H3K27ac) were performed using SimpleChIP plus kit (Cell Signaling) according to the manufacturer's instructions: chromatin preparations from eight-to-ten 15-cm dishes of preadipocytes or adipocytes (differentiated for 3 days) were pulled for each treatment/condition. Five μg of chromatin was used for each ChIP reaction that included either the negative control normal rabbit IgG (Cell Signaling #2729), PPARγ (81B8) rabbit mAb (Cell Signaling #2443), or acetyl-histone H3 (Lys27) (D5E4) XP rabbit mAb (Cell Signaling #8173). Eluted DNA samples were quantified using real-time PCR using primer pairs flanking two potential PPARγ binding sites on the 5' regulatory region of the *Lipe* or *Mgll* gene.

Indirect calorimetry. Monitoring of food intake, energy expenditure, and body temperature were performed in a Comprehensive Laboratory Animal Monitoring System (CLAMS, Columbus Instruments). Temperature probes were implanted subcutaneously one week prior to the experiment. Mice were individually housed and experiments were recorded continuously with ambient housing temperature for three days at thermoneutrality (30°C), three days at room temperature (22°C), and three days of cold (4°C).

CL 316,243 injection and signaling. Mice were administered CL 316,243 (CL, Tocris) in PBS at a dose of 1 mg/kg body weight via intraperitoneal injection. Injections were performed once daily for 7-10 days. Mice were weighed every 2 days, and the dose of CL was adjusted accordingly. For ex vivo signaling, inguinal fat pads were isolated from 20-week-old mice and sliced bidirectionally using a brain slicer. The minced tissue was pooled by genotypes, divided into 4 wells, and suspended in high-glucose DMEM. The tissue was acclimated for 10 minutes at 37°C with gentle shaking. CL (1 μM) was added for 0, 20, 40, and 60 minutes, after which tissue samples were washed with PBS and snap-frozen before processing for immunoblot analyses.

Triglyceride assay. Immortalized preadipocytes were plated and differentiated in 24-well plates. On day 6 of differentiation, cells were washed with PBS and lysed using a buffer containing 50 mM Tris, 100 mM NaCl, and 0.1% NP40. Lysates were used to assess triglyceride (TG) content with the Infinity Triglyceride kit (Thermo Scientific). TG content was normalized to total protein for each well.

Glucose tolerance test. Mice were subjected to an overnight fast, and fasting blood glucose was measured. Glucose in PBS was administered via intraperitoneal injection at a dose of 1.5 mg/kg body weight. Blood glucose concentration was measured at 15, 30, 45, 60, 90, and 120 minutes using a glucometer.

Histology. Longitudinal sections of adipose tissue were collected and fixed in Bouin's solution. . Tissue was embedded in paraffin, sectioned, and stained for hematoxylin and eosin (performed at

the Dana Farber Rodent Histopathology Core Facility). Section images were captured using the EVOS Cell Imaging System (ThermoFisher Scientific).

GWAS. The associations of genetic variants located at *IL13RA1*, *IL13RA2,* and *IL4R* with BMI and T2D were acquired from GWAS summary statistics made available from published studies conducted in the Biobank Japan (for both BMI and T2D) (34, 35), the Genetic Investigation of Anthropomorphic Traits (GIANT) Consortium (for BMI) (48), and the Diabetes Genetics Replication and Meta-analysis (DIAGRAM) Consortium (for T2D adjusted for BMI) (49). Regional association plots were generated using LocusZoom (66). Figure on tissue-specific gene expression (in subcutaneous and visceral adipose tissues, liver, and muscle) were generated using the GTEx Portal (50).

Statistical Analysis. All data are presented as mean ±SEM. Statistical analyses were performed using GraphPad Prism 7, with the exception of RNA-sequencing. Unpaired t-testing was used for comparison of two parameters. One-way ANOVA with Tukey's multiple comparisons test was used for analysis of *in vitro* experiments with more than 2 treatment conditions. Two-way ANOVA with Tukey's multiple comparisons test was used for analysis of *in vitro* experiments with 2 independent variables. Two-way ANOVA was used for evaluation of cold tolerance tests and GTT. Most Cell-based experiments were repeated 2-4 times. RNA-sequencing and validation of RNA sequencing in shIl13ra1 and Il13ra1RE cell lines were performed 1-2 times. Cell-based experiments were performed with 3-10 replicates, as noted in the figure legends.

Study approval. All animal studies were approved by the Harvard Medical Area Standing Committee on Animal Research and Academia Sinica Institutional Animal Care and Use Committee (IACUC: 23-10-2066 for Il4KO mice and neutralizing antibody studies).

Data availability. The complete RNA-Sequencing datasets have been deposited in the Gene Expression Omnibus database under accession number GSE171617. Gene lists for ontology analyses of differentiated adipocytes and preadipocytes are available in Supplemental Dataset 1 and Dataset 2, respectively. Values for all data points shown in graphs of the main and supplemental figures are presented in the Supporting data values XLS file.

Author Contributions

A.R.Y., M.M.C., N.H.K., A.L.H, J.P., H.C. Y.H.L. C.W.L and K.A.S. performed the experiments. A.L.H., N.H.K, M.M.C, and A.R.Y contributed to methods optimization and development of reagents. J.L and F.B.H. surveyed genetic associations from published GWAS and gene expression in human tissues in the GTEx Portal. A.S.B. oversaw CLAMS studies and provided feedback on data interpretation. J.S.L provided Il4KO mouse cohorts and D.Y.T and H.W.H conducted Il4KO-related experiments . A.R.Y, M.M.C, and C.H.L. conceptualized the study, designed experiments, and interpreted results. A.R.Y. and C.H.L wrote the manuscript. A.R.Y. and M.M.C are listed as co-first authors due to their shared contributions to the project. A.R.Y wrote and organized the manuscript and is therefore listed first amongst the two co-authors.

Acknowledgements

We thank Dr. Karen Inouye for comments and help with metabolic cage data interpretation, the IMB Genomics Core and Bioinformatics Service Core of the Academia Sinica for performing RNA-sequencing and raw data processing/analysis, and the Dana Farber Rodent Histopathology Core Facility for the sectioning and staining of adipose tissue. This work was supported by NIH predoctoral fellowship F31 DK125004 (A.R.Y) and F30 DK128884 (M.M.C) and a gift grant (A World without Diabetes) to C.H.L.

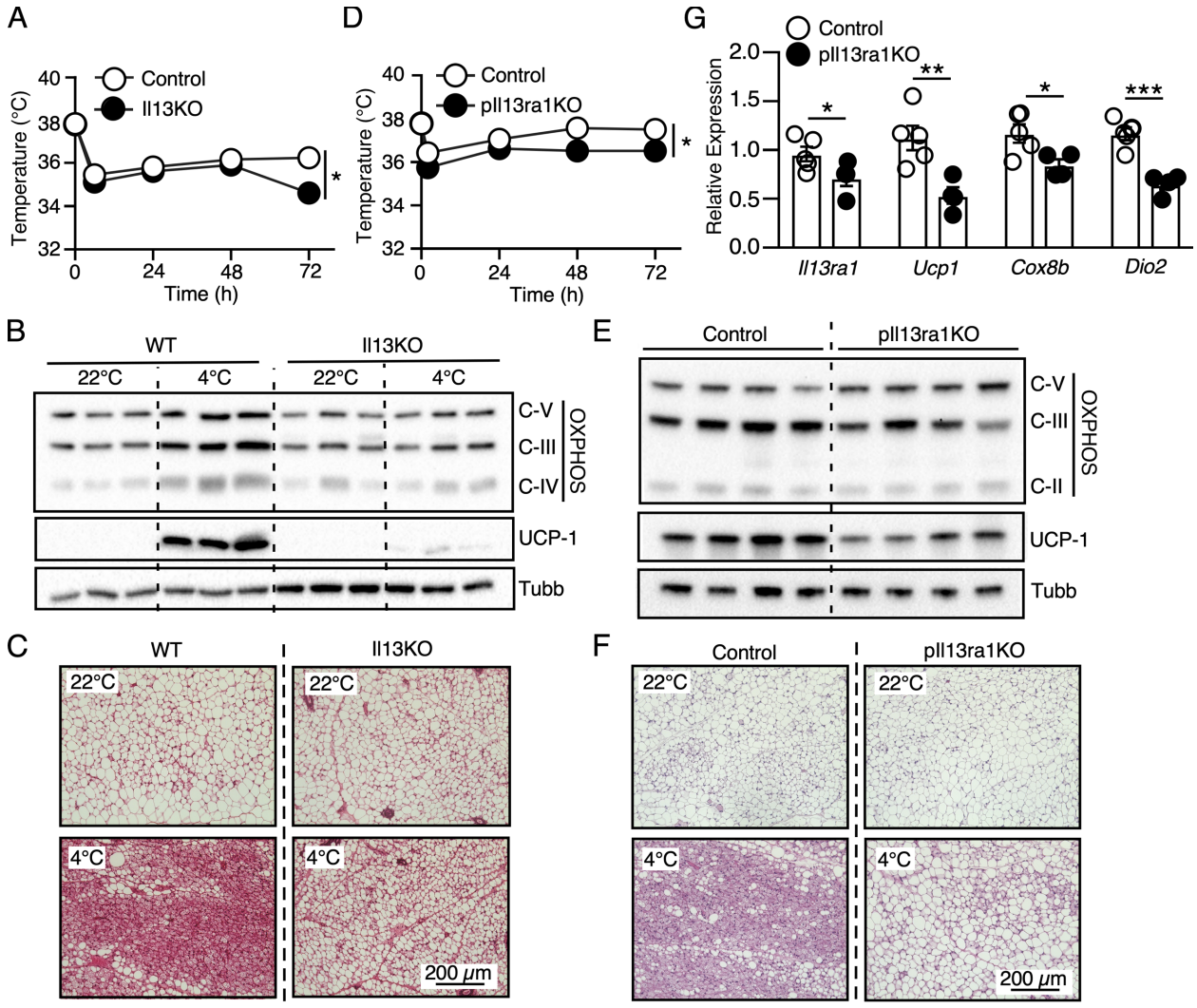

Figure 1. IL-13/IL-13Rα1 regulates beige adipocyte recruitment. (**A**) Core body temperature of WT and Il13KO mice during a 72-hour cold challenge at 4°C. n=6 WT and 5 Il13KO, 8-week-old female mice, 2-way ANOVA. Experiment repeated in two separate cohorts. (**B**) Immunoblots showing protein levels of UCP1 and mitochondrial OXPHOS complexes III (UQCRC2), IV (MTCO1), and V (ATP5A) in iWAT of WT and Il13KO mice. Representative samples from 3 mice/group are shown. (**C**) Representative H&E staining of iWAT from mice in (A). (**D**) Core body temperature of control and pIl13ra1KO mice during cold challenge at 4°C. n=5/group, 5-7-week-old male mice, 2-way ANOVA. Experiment performed in one cohort. (**E**) Immunoblots showing protein levels of UCP1 and mitochondrial OXPHOS complexes V, III, and II in iWAT of control and pIl13ra1KO mice after cold exposure in (D). Representative samples from 4 mice/group are shown. (**F**) Representative H&E staining of iWAT and (**G**) mRNA expression of *Il13ra1* and thermogenic genes measured by RT-qPCR in subcutaneous adipose tissue of cold-exposed control and pIl13ra1KO mice in (D). n=5/group, unpaired t-test. Values presented as mean ± SEM. *p<0.05, **p<0.01, ***p<0.001.

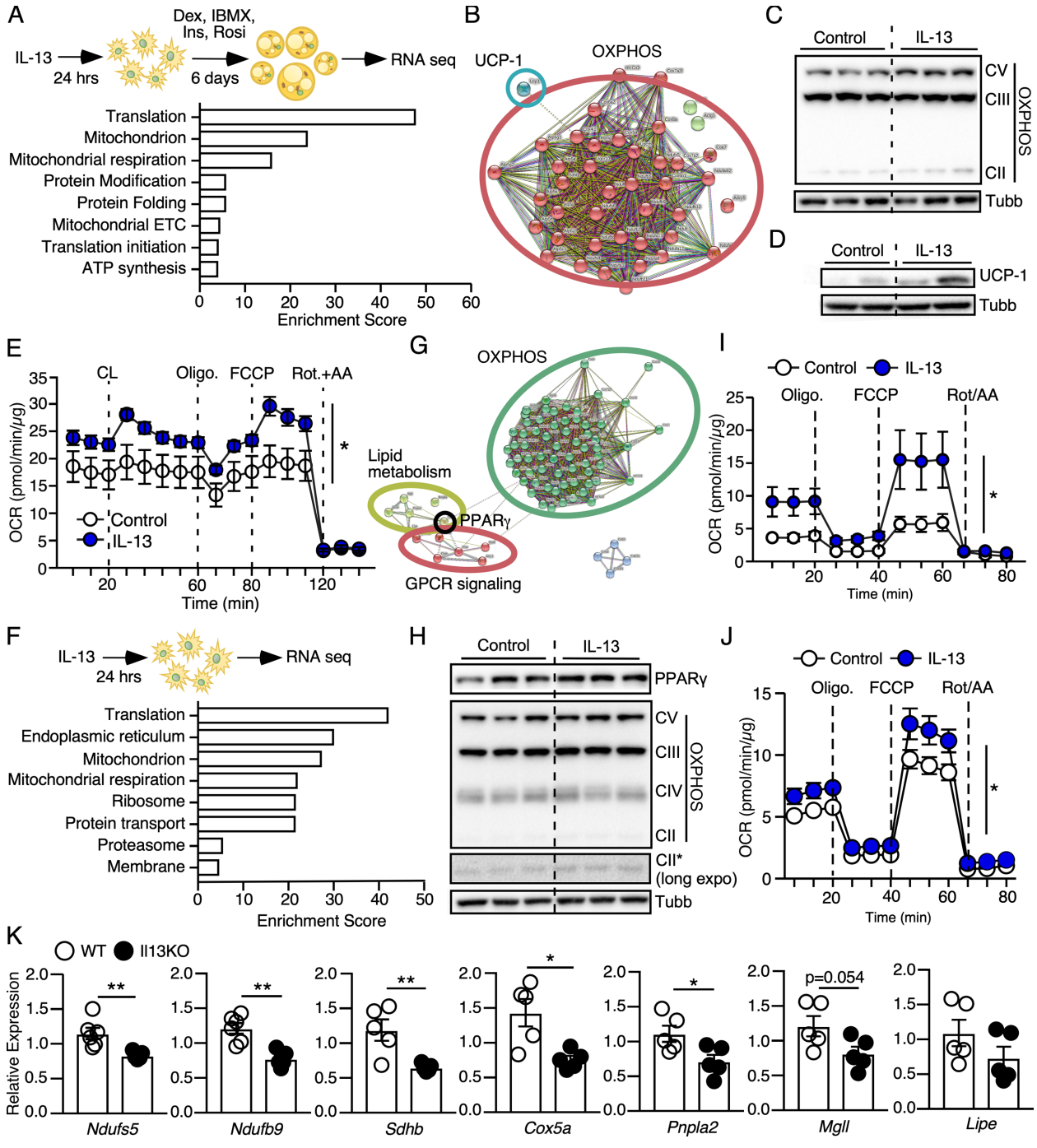

Figure 2. Regulation of mitochondrial-related metabolic programs by IL-13 in preadipocytes enhances the oxidative capacity of mature adipocytes. (**A**) Top: Schematic of cell treatments for RNA-sequencing analysis. WT clone B6 (referred to as WT) preadipocytes were treated with IL-13 or vehicle for 24 hours before induction of differentiation with dexamethasone (Dex), insulin (Ins), 3-isobutyl-1-methylxanthine (IBMX), and rosiglitazone (rosi) for 6 days. mRNA was isolated from differentiated adipocytes for sequencing. Bottom: Top enriched categories upregulated by IL-13 pretreatment in functional annotation analysis by DAVID. RNA-seq analysis performed once but

repeated in a separate clonal line. n=4, see Methods for statistical analysis. (**B**) STRING protein-protein interaction map of genes in the KEGG thermogenesis pathway upregulated by IL-13 pretreatment. Full list of genes in Supplemental Dataset 1. (**C**) Immunoblotting of mitochondrial OXPHOS complex II, III, and V proteins in WT adipocytes (n=3, 3-day differentiation, experiment repeated twice) and (**D**) UCP1 protein in mature WT adipocytes (n=2, 6-day differentiation) with or without IL-13 pretreatment. (**E**) Mitochondrial respiration of mature WT adipocytes with/without IL-13 pretreatment. CL 316,243 (CL) stimulated uncoupled respiration. Oligomycin (Oligo) inhibited coupled respiration. Trifluoromethoxy carbonylcyanide phenylhydrazone (FCCP) promoted maximal respiration. Rotenone and antimycin A (Rot/AA) inhibited mitochondrial respiration. n=10, experiment repeated 3 times, 2-way ANOVA. (**F**) Top: Schematic of cell treatments for RNA-sequencing analysis. WT preadipocytes were treated with IL-13 or vehicle for 24 hours, followed by RNA sequencing. Bottom: Top enriched categories upregulated by IL-13 in functional annotation analysis n=4. Full list of enriched categories in Supplemental Dataset 2. (**G**) STRING protein-protein interaction map of genes in the KEGG thermogenesis pathway upregulated by IL-13 treatment in preadipocytes. Full list of genes in Supplemental Dataset 2. (**H**) Immunoblotting showing protein levels of PPARγ and mitochondrial OXPHOS complexes II, III, IV, and V by IL-13 in WT preadipocytes. n=3/group, experiment repeated more than 3 times. (**I**) Mitochondrial respiration of WT preadipocytes treated with IL-13 for 24-hours. n=5, experiment repeated 3 times, 2-way ANOVA. (**J**) Mitochondrial respiration of primary preadipocytes treated with IL-13 for 24-hours. N=10, experiment repeated 2 times, 2-way ANOVA. (**K**) RT-qPCR analyses to assess the expression of OXPHOS genes and PPARγ target genes in iWAT of WT and Il13KO mice. n=6 WT and 5 Il13KO, 8-week-old female mice, unpaired t-test. *$p<0.05$, **$p<0.01$.

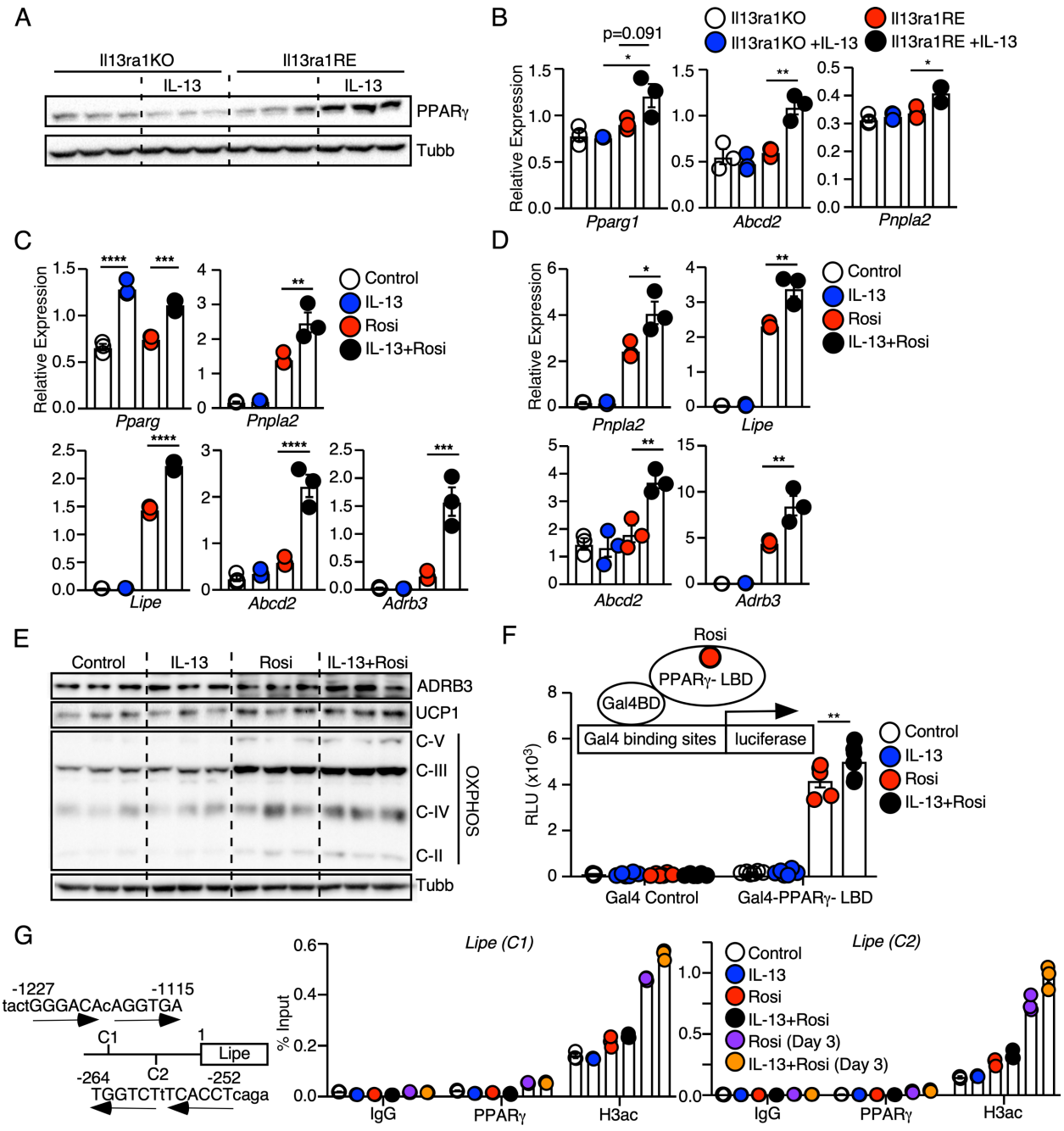

Figure 3. IL-13 potentiates PPARγ-mediated beige adipogenesis. (**A**) Immunoblot analysis of PPARγ protein in Il13ra1KO control and Il13ra1RE preadipocytes treated with IL-13 for 24 hours compared to untreated controls. n=3, experiment repeated twice. (**B**) RT-qPCR analyses of *Pparg1* and PPARγ target genes in Il13ra1KO control and Il13ra1RE preadipocytes treated with/without IL-13 for 24 hours. n=3, experiment performed 3 times, 2-way ANOVA with Tukey's multiple comparisons test. (**C**) RT-qPCR analyses of *Pparg* and PPARγ target genes in WT preadipocytes treated with vehicle, IL-13, rosi, or IL-13+rosi for 24 hours. n=3, experiment performed 4 times, one-way ANOVA with Tukey's multiple comparisons test. (**D**) RT-qPCR analyses in WT cells treated with vehicle, IL-13, rosi, or IL-13+rosi for 24 hours, followed by 2-day differentiation with

Dex, Ins, and IBMX. n=3, experiment performed 3 times, one-way ANOVA with Tukey's multiple comparisons test. (**E**) Immunoblot analysis of UCP1, ADRB3, and OXPHOS complexes in WT cells treated with vehicle, IL-13, rosi, or IL-13+rosi for 24 hours, followed by differentiation for 5 days with Dex, Ins and IBMX. n=3 /condition, experiment repeated twice. (**F**) Left: Schematic of the mammalian one-hybrid system. PPARγ ligand binding domain (LBD) was fused to yeast Gal4 DNA-binding domain (Gal4BD). WT preadipocytes were transfected with Gal4-Control or Gal4-PPARγ-LBD expression vector, together with Gal4 binding site containing luciferase report and β-galactosidase internal control. Right: Quantification of PPARγ-LBD transactivation activity on the luciferase reporter in preadipocytes treated with control, IL-13, rosi, or IL-13+rosi for 24 hours. Luciferase activity was measured 48 hours after transfection and normalized to β-galactosidase activity to determine the relative luciferase unit (RLU). n=4, experiment performed 3 times. (**G**) Left panel: Two sets of ChIP primer pairs (C1 and C2) were designed around two potential PPARγ binding sites (PPREs) in the 5' regulatory region of the *Lipe* gene. The transcriptional start site is designated as 1. Arrows indicate two direct repeat motifs of the PPRE. Right panel: Chromatin immunoprecipitation was performed on preadipocytes treated overnight with IL-13, rosi, or IL-13+rosi and on adipocytes differentiated for three days after overnight rosi or IL-13+rosi pretreatment. Protein-DNA complexes were pulled down using antibodies for IgG control, PPARγ, or acetylated histone H3 (H3ac, H3K27ac). RT-qPCR was performed using C1 and C2 primer pairs. n=3 technical replicates per condition, experiment performed 3 times. *$p<0.05$, **$p<0.01$, ***$p<0.001$, ****$p<0.0001$.

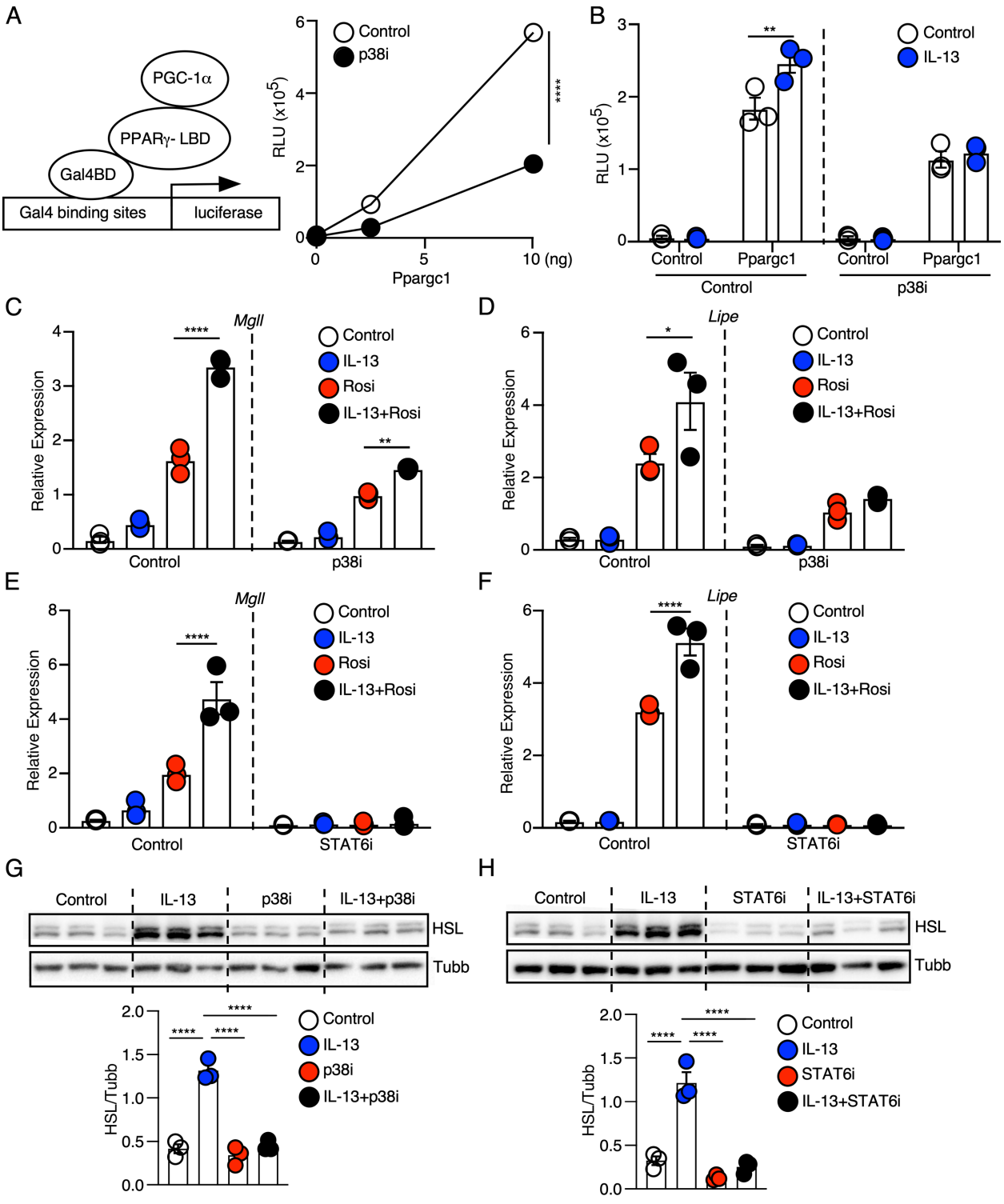

Figure 4. IL-13-IL-13Rα1 increases the expression and activity of PPARγ through STAT6 and p38 MAPK. (**A**) Left: Schematic of the one-hybrid system to assess PGC-1α coactivation on PPARγ-LBD activity. AD293 cells were transfected with Gal4-PPARγ-LBD and *Ppargc1* expression vector, together with Gal4 binding site containing luciferase reporter and β-galactosidase

internal control. Right: Quantification of PPARγ-LBD transactivation activity on luciferase reporter in AD293 cells co-transfected with 0, 2.5, and 10 ng of *Ppargc1a* expression vector in the presence of vehicle or P38 inhibitor (P38i, 10 μM). Luciferase activity was measured 48 hours after transfection and normalized to β-galactosidase activity to determine the relative luciferase units (RLU). n=3, experiment performed 3 times, 2-way ANOVA. (**B**) Quantification of PPARγ-LBD transactivation activity in AD293 cells co-transfected with luciferase/β-galactosidase reporters, Gal4-PPARγ-LBD and control vector or *Ppargc1a* expression vector (10 ng). Cells were treated with vehicle, IL-13, P38i, or IL-13+P38i overnight. RLU was determined 48 hours after transfection. n=3, experiment performed 3 times, 2-way ANOVA. (**C**) and (**D**) Expression of PPARγ target genes measured by RT-qPCR in WT preadipocytes treated with IL-13, rosi, or IL-13+rosi for 24 hours ± P38i. n=3, experiment performed two times, 2-way ANOVA with Tukey's multiple comparisons test. (**E**) and (**F**) Expression of PPARγ target genes by RT-qPCR in WT preadipocytes treated with IL-13, rosi, or IL-13+rosi for 24 hours ± STAT6 inhibitor (STAT6i, 10 μM). n=3, experiment performed once, 2-way ANOVA with Tukey's multiple comparisons test. (**G**) Immunoblotting showing HSL protein in preadipocytes treated with rosi plus IL-13 or vehicle ± P38i for 24 hours. n=3 with quantifications shown below, experiment performed twice. (**H**) Immunoblotting showing HSL protein in WT preadipocytes treated with rosi plus IL-13 or vehicle ± STAT6i for 24 hours. n=3 with quantifications shown below, experiment performed twice, one-way ANOVA with Tukey's multiple comparisons test. *p<0.05, **p<0.01, ***p<0.001, ****p<0.0001.

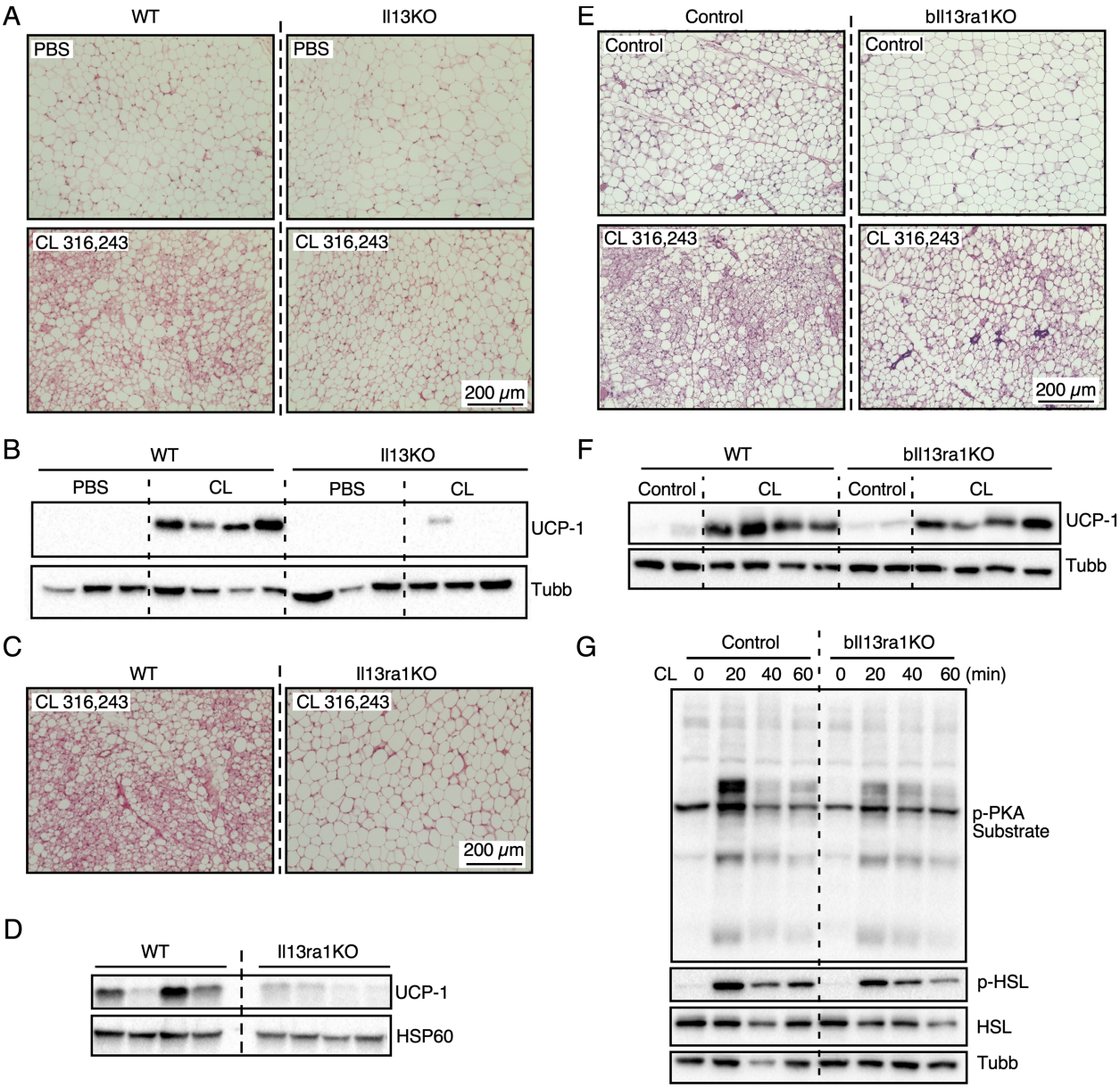

Figure 5. Adult mice deficient in IL-13 signaling exhibit impaired responses to β3-adrenergic stimulation. (**A**) Representative H&E staining of iWAT from WT and Il13KO mice injected with PBS or CL for 10 days. n=3-4/group, 3-month-old males. Experiment performed once. (**B**) Immunoblotting showing UCP1 protein levels in iWAT of WT and Il13KO mice in (A). Tubb: tubulin as a loading control. (**C**) H&E staining and (**D**) Immunoblotting of iWAT from control and Il13ra1KO mice injected with CL for 10 days. n=4, 30-week-old male mice. For H&E, samples from one mouse for each group were shown, with HSP60 as a loading control. (**E**) H&E staining and (**F**) Immunoblotting of iWAT from control and bIl13ra1KO mice injected with/without CL for 7 days. n=3 for non-injected controls and n=6-7 for CL injection, 5-month-old females. Experiment performed once. Representative tissue samples are shown. (**G**) Immunoblotting for HSL, phospho-HSL (S660), and phospho-PKA substrates in iWAT explants from control and bIl13ra1KO mice.

Tissue was stimulated with CL for 0, 20, 40, and 60 minutes ex vivo. Pooled analysis of 2 mice/genotype 5-month-old females, experiment performed 3 times.

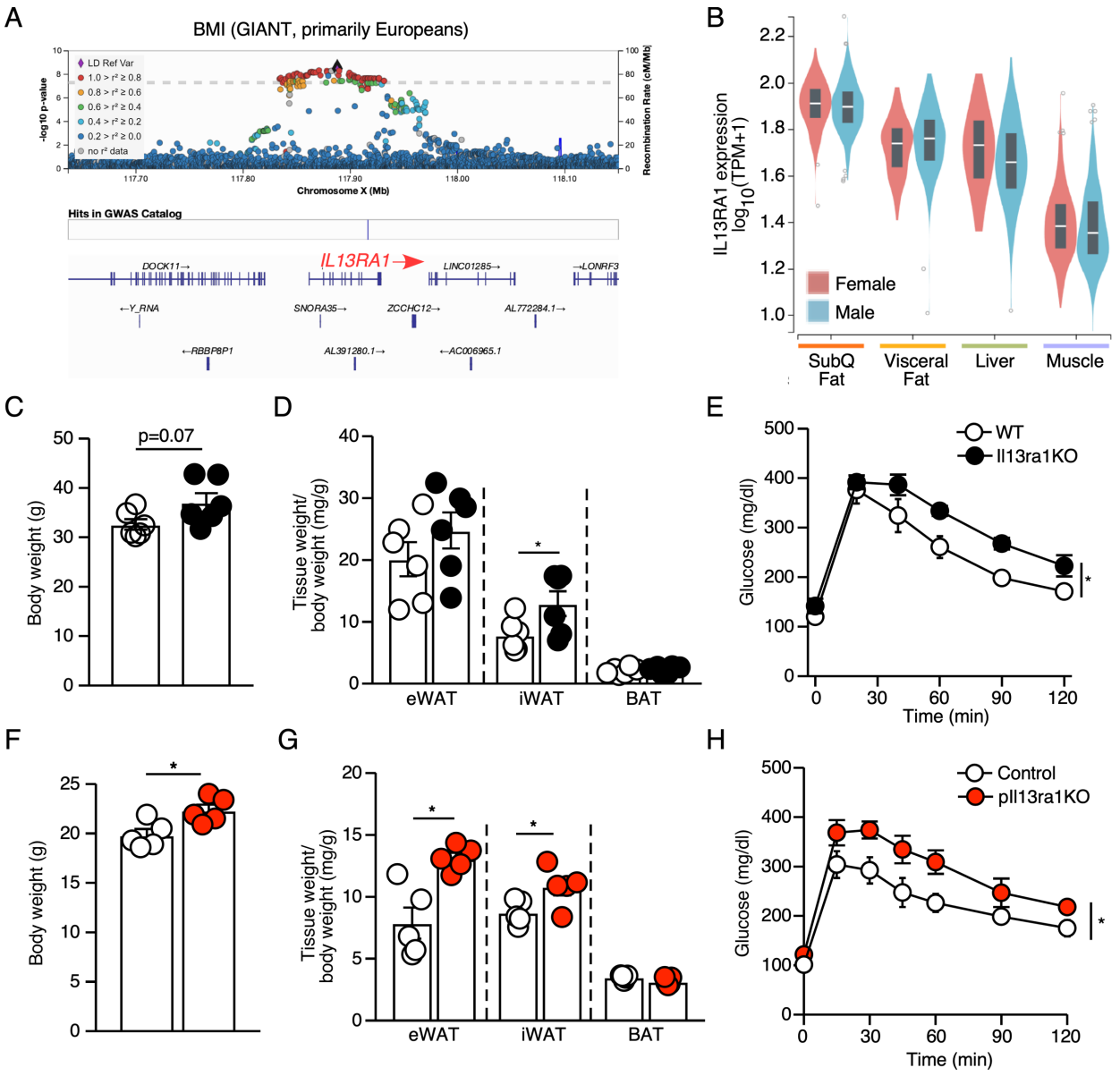

Figure 6. Il13ra1 is associated with body weight. (**A**) Variants located at *IL13RA1* gene showing genome-wide significant associations with BMI in a multi-ethnic population, based on X chromosome GWAS results from a GIANT (Genetic Investigation of Anthropomorphic Traits) Consortium study. The regional association plot was generated by Locuszoom (https://my.locuszoom.org/) on -log10 p-values for variant-trait associations. Each dot is a variant; the diamond shaped dot indicates the lead variant with the smallest p value. Dot colors indicate LD relationships (r^2) between all variants and the lead variants. Minor allele frequency (MAF) was not included. (**B**) Gene expression levels of *IL13RA1* (log transformed transcript per million) in 4 human tissues, in women and men, based on data from GTEx Portal. (**C**) Body weight and (**D**) Fat tissue weight normalized to body weight of WT and Il13ra1KO mice. n=6/genotype, 20-week-old males, unpaired t-test. (**E**) Intraperitoneal glucose tolerance test (GTT) of WT and Il13ra1KO mice. N=5-6 per group, 5-month-old mice, 2-way ANOVA. C-E repeated in two separate cohorts. (**F**)

Body weight and (**G**) Fat tissue weight normalized to body weight of control and pIl13ra1KO mice. N=5/group, 5-7-week-old males, unpaired t-test. (**H**) GTT of WT and pIl13ra1KO mice. n=7/group, 20-week-old females, experiment performed in one cohort, 2-way ANOVA. *$p<0.05$.

References

1. Larsson SC, and Burgess S. Causal role of high body mass index in multiple chronic diseases: a systematic review and meta-analysis of Mendelian randomization studies. *BMC Med.* 2021;19(1):320.
2. Bartelt A, and Heeren J. Adipose tissue browning and metabolic health. *Nat Rev Endocrinol.* 2014;10(1):24-36.
3. Kajimura S, Spiegelman BM, and Seale P. Brown and Beige Fat: Physiological Roles beyond Heat Generation. *Cell Metab.* 2015;22(4):546-59.
4. Zhang F, Hao G, Shao M, Nham K, An Y, Wang Q, et al. An Adipose Tissue Atlas: An Image-Guided Identification of Human-like BAT and Beige Depots in Rodents. *Cell Metab.* 2018;27(1):252-62 e3.
5. Saito M, Okamatsu-Ogura Y, Matsushita M, Watanabe K, Yoneshiro T, Nio-Kobayashi J, et al. High incidence of metabolically active brown adipose tissue in healthy adult humans: effects of cold exposure and adiposity. *Diabetes.* 2009;58(7):1526-31.
6. van Marken Lichtenbelt WD, Vanhommerig JW, Smulders NM, Drossaerts JM, Kemerink GJ, Bouvy ND, et al. Cold-activated brown adipose tissue in healthy men. *N Engl J Med.* 2009;360(15):1500-8.
7. Cypess AM, Lehman S, Williams G, Tal I, Rodman D, Goldfine AB, et al. Identification and importance of brown adipose tissue in adult humans. *N Engl J Med.* 2009;360(15):1509-17.
8. Finlin BS, Memetimin H, Zhu B, Confides AL, Vekaria HJ, El Khouli RH, et al. The beta3-adrenergic receptor agonist mirabegron improves glucose homeostasis in obese humans. *J Clin Invest.* 2020;130(5):2319-31.

9. Sharp LZ, Shinoda K, Ohno H, Scheel DW, Tomoda E, Ruiz L, et al. Human BAT possesses molecular signatures that resemble beige/brite cells. *PLoS One.* 2012;7(11):e49452.

10. Wu J, Bostrom P, Sparks LM, Ye L, Choi JH, Giang AH, et al. Beige adipocytes are a distinct type of thermogenic fat cell in mouse and human. *Cell.* 2012;150(2):366-76.

11. Wang QA, Tao C, Gupta RK, and Scherer PE. Tracking adipogenesis during white adipose tissue development, expansion and regeneration. *Nat Med.* 2013;19(10):1338-44.

12. Harms M, and Seale P. Brown and beige fat: development, function and therapeutic potential. *Nat Med.* 2013;19(10):1252-63.

13. Shao M, Wang QA, Song A, Vishvanath L, Busbuso NC, Scherer PE, et al. Cellular Origins of Beige Fat Cells Revisited. *Diabetes.* 2019;68(10):1874-85.

14. Cho DS, Lee B, and Doles JD. Refining the adipose progenitor cell landscape in healthy and obese visceral adipose tissue using single-cell gene expression profiling. *Life Sci Alliance.* 2019;2(6).

15. Oguri Y, Shinoda K, Kim H, Alba DL, Bolus WR, Wang Q, et al. CD81 Controls Beige Fat Progenitor Cell Growth and Energy Balance via FAK Signaling. *Cell.* 2020;182(3):563-77 e20.

16. Rondini EA, and Granneman JG. Single cell approaches to address adipose tissue stromal cell heterogeneity. *Biochem J.* 2020;477(3):583-600.

17. Schwalie PC, Dong H, Zachara M, Russeil J, Alpern D, Akchiche N, et al. A stromal cell population that inhibits adipogenesis in mammalian fat depots. *Nature.* 2018;559(7712):103-8.

18. Shapira SN, and Seale P. Transcriptional Control of Brown and Beige Fat Development and Function. *Obesity (Silver Spring).* 2019;27(1):13-21.

19. Fu M, Sun T, Bookout AL, Downes M, Yu RT, Evans RM, et al. A Nuclear Receptor Atlas: 3T3-L1 adipogenesis. *Mol Endocrinol.* 2005;19(10):2437-50.

20. Petrovic N, Walden TB, Shabalina IG, Timmons JA, Cannon B, and Nedergaard J. Chronic peroxisome proliferator-activated receptor gamma (PPARgamma) activation of epididymally derived white adipocyte cultures reveals a population of thermogenically competent, UCP1-containing adipocytes molecularly distinct from classic brown adipocytes. *J Biol Chem.* 2010;285(10):7153-64.

21. Ohno H, Shinoda K, Spiegelman BM, and Kajimura S. PPARgamma agonists induce a white-to-brown fat conversion through stabilization of PRDM16 protein. *Cell Metab.* 2012;15(3):395-404.

22. Hepler C, Vishvanath L, and Gupta RK. Sorting out adipocyte precursors and their role in physiology and disease. *Genes Dev.* 2017;31(2):127-40.

23. Wu Y, Kinnebrew MA, Kutyavin VI, and Chawla A. Distinct signaling and transcriptional pathways regulate peri-weaning development and cold-induced recruitment of beige adipocytes. *Proc Natl Acad Sci U S A.* 2020;117(12):6883-9.

24. Chi J, Lin Z, Barr W, Crane A, Zhu XG, and Cohen P. Early postnatal interactions between beige adipocytes and sympathetic neurites regulate innervation of subcutaneous fat. *Elife.* 2021;10.

25. Lee MW, Odegaard JI, Mukundan L, Qiu Y, Molofsky AB, Nussbaum JC, et al. Activated type 2 innate lymphoid cells regulate beige fat biogenesis. *Cell.* 2015;160(1-2):74-87.

26. Roh HC, Tsai LTY, Shao M, Tenen D, Shen Y, Kumari M, et al. Warming Induces Significant Reprogramming of Beige, but Not Brown, Adipocyte Cellular Identity. *Cell Metab.* 2018;27(5):1121-37 e5.

27. Rosenwald M, Perdikari A, Rulicke T, and Wolfrum C. Bi-directional interconversion of brite and white adipocytes. *Nat Cell Biol.* 2013;15(6):659-67.

28. McCormick SM, and Heller NM. Commentary: IL-4 and IL-13 receptors and signaling. *Cytokine.* 2015;75(1):38-50.

29. Walker JA, and McKenzie ANJ. T(H)2 cell development and function. *Nat Rev Immunol.* 2018;18(2):121-33.

30. Brestoff JR, Kim BS, Saenz SA, Stine RR, Monticelli LA, Sonnenberg GF, et al. Group 2 innate lymphoid cells promote beiging of white adipose tissue and limit obesity. *Nature.* 2015;519(7542):242-6.

31. Qiu Y, Nguyen KD, Odegaard JI, Cui X, Tian X, Locksley RM, et al. Eosinophils and type 2 cytokine signaling in macrophages orchestrate development of functional beige fat. *Cell.* 2014;157(6):1292-308.

32. Knudsen NH, Stanya KJ, Hyde AL, Chalom MM, Alexander RK, Liou YH, et al. Interleukin-13 drives metabolic conditioning of muscle to endurance exercise. *Science.* 2020;368(6490).

33. Stanya KJ, Jacobi D, Liu S, Bhargava P, Dai L, Gangl MR, et al. Direct control of hepatic glucose production by interleukin-13 in mice. *J Clin Invest.* 2013;123(1):261-71.

34. Suzuki K, Akiyama M, Ishigaki K, Kanai M, Hosoe J, Shojima N, et al. Identification of 28 new susceptibility loci for type 2 diabetes in the Japanese population. *Nat Genet.* 2019;51(3):379-86.

35. Akiyama M, Okada Y, Kanai M, Takahashi A, Momozawa Y, Ikeda M, et al. Genome-wide association study identifies 112 new loci for body mass index in the Japanese population. *Nat Genet.* 2017;49(10):1458-67.

36. Sanchez-Gurmaches J, Hsiao WY, and Guertin DA. Highly selective in vivo labeling of subcutaneous white adipocyte precursors with Prx1-Cre. *Stem Cell Reports.* 2015;4(4):541-50.

37. Huang da W, Sherman BT, and Lempicki RA. Systematic and integrative analysis of large gene lists using DAVID bioinformatics resources. *Nat Protoc.* 2009;4(1):44-57.

38. Sherman BT, Hao M, Qiu J, Jiao X, Baseler MW, Lane HC, et al. DAVID: a web server for functional enrichment analysis and functional annotation of gene lists (2021 update). *Nucleic Acids Res.* 2022.

39. Bi P, Shan T, Liu W, Yue F, Yang X, Liang XR, et al. Inhibition of Notch signaling promotes browning of white adipose tissue and ameliorates obesity. *Nat Med.* 2014;20(8):911-8.

40. Lee MJ, Jash S, Jones JEC, Puri V, and Fried SK. Rosiglitazone remodels the lipid droplet and britens human visceral and subcutaneous adipocytes ex vivo. *J Lipid Res.* 2019;60(4):856-68.

41. Merlin J, Sato M, Nowell C, Pakzad M, Fahey R, Gao J, et al. The PPARgamma agonist rosiglitazone promotes the induction of brite adipocytes, increasing beta-adrenoceptor-mediated mitochondrial function and glucose uptake. *Cell Signal.* 2018;42:54-66.

42. Wilson-Fritch L, Nicoloro S, Chouinard M, Lazar MA, Chui PC, Leszyk J, et al. Mitochondrial remodeling in adipose tissue associated with obesity and treatment with rosiglitazone. *J Clin Invest.* 2004;114(9):1281-9.

43. Vernochet C, Peres SB, Davis KE, McDonald ME, Qiang L, Wang H, et al. C/EBPalpha and the corepressors CtBP1 and CtBP2 regulate repression of select visceral white adipose genes during induction of the brown phenotype in white adipocytes by peroxisome proliferator-activated receptor gamma agonists. *Mol Cell Biol.* 2009;29(17):4714-28.

44. Puigserver P, Rhee J, Lin J, Wu Z, Yoon JC, Zhang CY, et al. Cytokine stimulation of energy expenditure through p38 MAP kinase activation of PPARgamma coactivator-1. *Mol Cell.* 2001;8(5):971-82.

45. Xu B, Bhattacharjee A, Roy B, Xu HM, Anthony D, Frank DA, et al. Interleukin-13 induction of 15-lipoxygenase gene expression requires p38 mitogen-activated protein kinase-mediated serine 727 phosphorylation of Stat1 and Stat3. *Mol Cell Biol.* 2003;23(11):3918-28.

46. Odegaard JI, Ricardo-Gonzalez RR, Goforth MH, Morel CR, Subramanian V, Mukundan L, et al. Macrophage-specific PPARgamma controls alternative activation and improves insulin resistance. *Nature.* 2007;447(7148):1116-20.

47. Szanto A, Balint BL, Nagy ZS, Barta E, Dezso B, Pap A, et al. STAT6 transcription factor is a facilitator of the nuclear receptor PPARgamma-regulated gene expression in macrophages and dendritic cells. *Immunity.* 2010;33(5):699-712.

48. Locke AE, Kahali B, Berndt SI, Justice AE, Pers TH, Day FR, et al. Genetic studies of body mass index yield new insights for obesity biology. *Nature.* 2015;518(7538):197-206.

49. Scott RA, Scott LJ, Magi R, Marullo L, Gaulton KJ, Kaakinen M, et al. An Expanded Genome-Wide Association Study of Type 2 Diabetes in Europeans. *Diabetes.* 2017;66(11):2888-902.

50. Mele M, Ferreira PG, Reverter F, DeLuca DS, Monlong J, Sammeth M, et al. Human genomics. The human transcriptome across tissues and individuals. *Science.* 2015;348(6235):660-5.

51. Shabalina IG, Petrovic N, de Jong JM, Kalinovich AV, Cannon B, and Nedergaard J. UCP1 in brite/beige adipose tissue mitochondria is functionally thermogenic. *Cell Rep.* 2013;5(5):1196-203.

52. Puigserver P, and Spiegelman BM. Peroxisome proliferator-activated receptor-gamma coactivator 1 alpha (PGC-1 alpha): transcriptional coactivator and metabolic regulator. *Endocr Rev.* 2003;24(1):78-90.

53. Kleiner S, Mepani RJ, Laznik D, Ye L, Jurczak MJ, Jornayvaz FR, et al. Development of insulin resistance in mice lacking PGC-1alpha in adipose tissues. *Proc Natl Acad Sci U S A.* 2012;109(24):9635-40.

54. Cao W, Daniel KW, Robidoux J, Puigserver P, Medvedev AV, Bai X, et al. p38 mitogen-activated protein kinase is the central regulator of cyclic AMP-dependent transcription of the brown fat uncoupling protein 1 gene. *Mol Cell Biol.* 2004;24(7):3057-67.

55. Masud S, Ye S, and Group SAS. Effect of the peroxisome proliferator activated receptor-gamma gene Pro12Ala variant on body mass index: a meta-analysis. *J Med Genet.* 2003;40(10):773-80.

56. Altshuler D, Hirschhorn JN, Klannemark M, Lindgren CM, Vohl MC, Nemesh J, et al. The common PPARgamma Pro12Ala polymorphism is associated with decreased risk of type 2 diabetes. *Nat Genet.* 2000;26(1):76-80.

57. Ahmadian M, Suh JM, Hah N, Liddle C, Atkins AR, Downes M, et al. PPARgamma signaling and metabolism: the good, the bad and the future. *Nat Med.* 2013;19(5):557-66.

58. Semple RK, Chatterjee VK, and O'Rahilly S. PPAR gamma and human metabolic disease. *J Clin Invest.* 2006;116(3):581-9.

59. Zhang Q, Shan B, Guo L, Shao M, Vishvanath L, Elmquist G, et al. Distinct functional properties of murine perinatal and adult adipose progenitor subpopulations. *Nat Metab.* 2022;4(8):1055-70.

60. Mohrs K, Wakil AE, Killeen N, Locksley RM, and Mohrs M. A two-step process for cytokine production revealed by IL-4 dual-reporter mice. *Immunity.* 2005;23(4):419-29.

61. Logan M, Martin JF, Nagy A, Lobe C, Olson EN, and Tabin CJ. Expression of Cre Recombinase in the developing mouse limb bud driven by a Prxl enhancer. *Genesis.* 2002;33(2):77-80.

62. Kong X, Banks A, Liu T, Kazak L, Rao RR, Cohen P, et al. IRF4 is a key thermogenic transcriptional partner of PGC-1alpha. *Cell.* 2014;158(1):69-83.

63. Bapat SP, Whitty C, Mowery CT, Liang Y, Yoo A, Jiang Z, et al. Obesity alters pathology and treatment response in inflammatory disease. *Nature.* 2022;604(7905):337-42.

64. Liou YH, Personnaz J, Jacobi D, Knudsen NH, Chalom MM, Starost KA, et al. Hepatic Fis1 regulates mitochondrial integrated stress response and improves metabolic homeostasis. *JCI Insight.* 2022;7(4).

65. Szklarczyk D, Gable AL, Nastou KC, Lyon D, Kirsch R, Pyysalo S, et al. The STRING database in 2021: customizable protein-protein networks, and functional characterization of user-uploaded gene/measurement sets. *Nucleic Acids Res.* 2021;49(D1):D605-D12.

66. Pruim RJ, Welch RP, Sanna S, Teslovich TM, Chines PS, Gliedt TP, et al. LocusZoom: regional visualization of genome-wide association scan results. *Bioinformatics.* 2010;26(18):2336-7.